

CORRELATION BETWEEN MASTER CURVES OBTAINED FROM
RHEOLOGY AND MECHANICAL TESTING

A THESIS SUBMITTED TO
THE GRADUATE SCHOOL OF NATURAL AND APPLIED SCIENCES
OF
MIDDLE EAST TECHNICAL UNIVERSITY

BY

AYŞE HANDE ŞARMAN

IN PARTIAL FULFILLMENT OF THE REQUIREMENTS
FOR
THE DEGREE OF MASTER OF SCIENCE
IN
CHEMISTRY

SEPTEMBER 2015

Approval of the thesis:

**CORRELATION BETWEEN MASTER CURVES OBTAINED FROM
RHEOLOGY AND MECHANICAL TESTING**

submitted by **AYŞE HANDE ŞARMAN** in partial fulfillment of the requirements
for the degree of **Master of Science in Chemistry Department, Middle East
Technical University** by,

Prof. Dr. Gülbin Dural Ünver
Dean, Graduate School of **Natural and Applied Sciences**

Prof. Dr. Cihangir Tanyeli
Head of Department, **Chemistry**

Prof. Dr. Teoman Tinçer
Supervisor, **Chemistry Department, METU**

Examining Committee Members:

Prof. Dr. Necati Özkan
Polymer Science and Technology Dept., METU

Prof. Dr. Teoman Tinçer
Chemistry Dept., METU

Prof. Dr. Ahmet M. Önal
Chemistry Dept., METU

Assoc. Prof. Dr. Ali Çırpan
Chemistry Dept., METU

Assist. Prof. Dr. Erhan Bat
Chemical Eng. Dept., METU

Date: 08.09.2015

I hereby declare that all information in this document has been obtained and presented in accordance with academic rules and ethical conduct. I also declare that, as required by these rules and conduct, I have fully cited and referenced all material and results that are not original to this work.

Name, Last Name: Ayşe Hande ŞARMAN

Signature:

ABSTRACT

CORRELATION BETWEEN MASTER CURVES OBTAINED FROM RHEOLOGY AND MECHANICAL TESTING

Şarman, Ayşe Hande

M. S., Department of Chemistry

Supervisor: Prof. Dr. Teoman Tinçer

August 2015, 114 pages

Characterization of viscoelastic materials has attracted attention since 1850s due to temperature dependent properties they perform. Time – temperature superposition principle is an important concept to estimate the behavior of viscoelastic materials. This principle is used to generate master curves for viscoelastic polymers by using time – temperature equivalence principle. There were mainly two techniques used in the recent studies. The most common characterization is mechanical testing and second technique is dynamic mechanical analysis (DMA). In this study, a HTPB (10-15%) based rocket propellant containing ammonium perchlorate (65-70%), aluminum powder (15-20%) was chosen and its master curves were estimated both with mechanical tests and rheometer. The aim was to compare the shift factors and master curves. At first, under certain frequency and temperature range the master curve was generated by rheometer. After that, shift factors and complex modulus were calculated.

On the other hand, stress relaxation tests were performed to determine relaxation modulus and shift factor at different temperatures. According to test results, master curve of the given propellant was generated by time – temperature superposition principle. Finally, the results obtained from both rheometer and stress relaxation

results were compared. For comparison, the complex modulus obtained from the rheometer was converted to relaxation modulus by taking the Poisson's ratio as 0.5. The shift factors and obtained master curves were compared for each technique. As a result, for the propellant, no correlation was obtained between the techniques and it was concluded that, mechanical tests cannot be replaced with rheometer tests.

Keywords: Rheometer, time – temperature superposition, rheology, propellant, master curve

ÖZ

REOMETRE VE MEKANİK TESTLER SONUCU ELDE EDİLEN ANA EĞRİLER ARASINDAKİ İLİŞKİ

Şarman, Ayşe Hande

Yüksek Lisans, Kimya Bölümü

Tez Yöneticisi: Prof. Dr. Teoman Tinçer

Ağustos 2015, 114 sayfa

Vizkoelastik malzemelerin karakterizasyonu, zorlu işlenebilirlik koşulları ve sıcaklıkla değişen özellikleri sebebiyle 1850'lerden beri önemli olmuştur. Zaman – sıcaklık eş değeri prensibi, vizkoelastik malzemelerin davranışlarını belirlemede kullanılan önemli bir prensiptir. Bu prensip sayesinde vizkoelastik malzemelerin ana eğri çalışmaları gerçekleştirilmiştir. Ana eğri oluşturulurken genellikle iki yöntem çalışılmaktadır. Birincisi mekanik testler ikincisi ise dinamik mekanik analizdir (DMA). Bu çalışmada, HTPB (10-15%) bazlı, amonyum perklorat (65-70%) ve alüminyum tozu (15-20%) içeren katı roket yakıtı seçilerek mekanik testlerle ve reometre cihazı ile ana eğri çıkarılmıştır. Çalışmada, iki yöntem ile elde edilen kaydırma fonksiyonu sabitleri ve ana eğrilerin karşılaştırılması amaçlanmıştır. Başlangıç olarak, belirli bir frekans ve sıcaklık aralığında kaydırma fonksiyonu sabiti ve kompleks modulus değerleri reometre ile hesaplanmıştır.

Ek olarak, farklı sıcaklıklarda gerinim – gevşeme testleri, gevşeme modülü ve kaydırma fonksiyonunu hesaplamak için gerçekleştirilmiştir. Bu sonuçlara göre, seçilen yakıtın ana eğri zaman sıcaklık eşdeğeri prensibine göre çıkarılmıştır.

Son olarak bu iki çalışmadan elde edilen sonuçlar karşılaştırılmıştır. Karşılaştırma yapılabilmesi için reometreden elde edilen kompleks modulus, Poisson oranı 0.5 alınarak gevşeme modülü cinsinden ifade edilmiştir. Her iki yöntem ile hesaplanan kaydırma fonksiyonu ve ana eğriler hesaplanmıştır. Sonuç olarak, iki teknik arasında tutarlı bir korelasyon kurulamamış ve ana eğri çıkarılması için mekanik testler yerine reometre testlerinin kullanılamayacağı sonucuna varılmıştır.

Anahtar Kelimeler: Reometre, zaman-sıcaklık eşdeğerliliği, reoloji, yakıt, ana eğri

To my beloved family

ACKNOWLEDGEMENT

I would like to present my feelings of gratitude to my supervisor Prof. Dr. Teoman TİNÇER and Prof. Dr. Necati ÖZKAN for their guidance, support and endless patience. It was a great pleasure to learn many issues about propellants, rheology and master curves.

I am very grateful to my company, ROKETSAN, especially to Materials and Ballistic Technologies Protection Department for supportive and understanding behavior throughout my master program.

I would like to thank to my department, High Temperature Material Characterization Laboratory, especially to Faruk YILDIRIM and Cengiz TETİK in ROKETSAN for supportive and helpful attitude.

I wish to express my thanks to Sibel ARAL in ROKETSAN for her help in my studies.

I would like to express my special thanks to all the members of my thesis examine committee for their valuable critics and help during my study.

The last but not the least, I would like to present my sincere appreciation to my sister Emine Hale YAĞLICI, my FAMILY and friends, especially to my fiancé Alper ÇALIŞ for their support. It would be very difficult to achieve this hard work without them.

TABLE OF CONTENTS

ABSTRACT.....	v
ÖZ	vii
ACKNOWLEDGEMENT	x
TABLE OF CONTENTS.....	xi
LIST OF TABLES	xvi
LIST OF FIGURES	xvii
LIST OF ABBREVIATIONS	xx
CHAPTERS	1
CHAPTER 1 INTRODUCTION	1
1.1 PROPELLANT CLASSIFICATION	2
1.1.1 LIQUID PROPELLANTS.....	2
1.1.2 SOLID PROPELLANTS.....	2
1.1.2.1 DOUBLE BASE – HOMOGENEOUS PROPELLANTS....	2
1.1.2.2 COMPOSITE – NON HOMOGENEOUS PROPELLANTS	3
1.2 INGREDIENTS OF A COMPOSITE PROPELLANT	5
1.2.1 MAIN ADDITIVES	5
1.2.1.1 BINDER	5
1.2.1.2 OXIDIZER	6
1.2.1.3 FUEL.....	6
1.2.2 OTHER ADDITIVES	7
1.2.2.1 PLASTICIZER.....	7
1.2.2.2 CURING AGENT	7

1.2.2.3	BONDING AGENT	7
1.2.2.4	BURNING RATE MODIFIERS	8
1.2.2.5	ANTI – OXIDANTS	8
1.3	PROPELLANT CHARACTERIZATION	9
1.4	CHARACTERIZATION CONCEPTS	12
1.4.1	THERMAL CHARACTERIZATION	12
1.4.1.1	AUTO IGNITION TEMPERATURE.....	12
1.4.1.2	SPECIFIC HEAT, C_p	12
1.4.1.3	COEFFICIENT OF LINEAR THERMAL EXPANSION, CTE.....	12
1.4.1.4	DECOMPOSITION TEMPERATURE	13
1.4.1.5	THERMAL CONDUCTIVITY.....	13
1.4.2	THERMAL CHARACTERIZATION METHODS	14
1.4.2.1	DIFFERENTIAL SCANNING CALORIMETRY (DSC)..	14
1.4.2.2	THERMO MECHANICAL ANALYZER (TMA)	15
1.4.2.3	THERMOGRAVIMETRIC ANALYZER (TGA).....	17
1.4.2.4	THERMAL CONDUCTIVITY.....	18
1.4.3	RHEOLOGICAL CHARACTERIZATION	20
1.4.3.1	RHEOLOGY	20
1.4.3.2	TERMS AND CONCEPTS.....	20
1.4.3.3	UNDERSTANDING VISCOELASTIC BEHAVIOR.....	22
1.4.3.4	MAXWELL MODEL	22
1.4.3.5	VOIGHT – KELVIN MODEL.....	23
1.4.3.6	GENERALIZED MODELS	25
1.4.4	RHEOLOGICAL CHARACTERIZATION PARAMETERS.....	26

1.4.4.1	MODULUS	26
1.4.4.2	GLASS TRANSITION TEMPERATURE, T_g	29
1.4.5	RHEOMETERS	30
1.4.6	DYNAMIC MECHANICAL ANALYZER (DMA).....	32
1.4.7	MECHANICAL CHARACTERIZATION	34
1.4.8	TIME – TEMPERATURE SUPERPOSITION AND MASTER CURVES	35
1.4.8.1	WHAT IS A MASTER CURVE?	35
1.4.8.2	THE TIME – TEMPERATURE SUPERPOSITION:	35
1.4.8.3	TTS VALIDITY.....	39
1.4.8.4	ARRHENIUS RELATION AND ACTIVATION ENERGY	41
1.4.8.5	DETERMINATION OF MASTER CURVE BY RHEOMETER	42
1.4.8.6	DETERMINATION OF MASTER CURVE BY MECHANICAL TESTING.....	43
1.4.8.7	COMPARISON OF MASTER CURVES.....	44
1.5	LITERATURE REVIEW.....	45
1.6	AIM OF THE STUDY	48
CHAPTER 2 EXPERIMENTAL.....		51
2.1	CHEMICALS	51
2.2	PREPARATION OF THE PROPELLANT MIXTURE.....	51
2.3	PREPARATION OF PROPELLANT SAMPLES FOR TESTS	52
2.4	PROPELLANT CHARACTERIZATION	55
2.4.1	THERMAL CHARACTERIZATION	55
2.4.1.1	AUTOIGNITION TEMPERATURE.....	55

2.4.1.2	SPECIFIC HEAT, C_p	58
2.4.1.3	THERMAL CONDUCTIVITY	59
2.4.1.4	COEFFICIENT OF LINEAR THERMAL EXPANSION, CTE.....	61
2.4.1.5	DECOMPOSITION TEMPERATURE	62
2.4.2	RHEOLOGICAL CHARACTERIZATION	64
2.4.2.1	GLASS TRANSITION TEMPERATURE, T_g	64
2.5	DETERMINATION OF MASTER CURVE BY RHEOMETER	65
2.6	DETERMINATION OF MASTER CURVE BY UNIVERSAL MECHANICAL TEST SYSTEM	66
CHAPTER 3	RESULTS AND DISCUSSION	71
3.1	DETERMINATION OF AUTOIGNITION TEMPERATURE.....	72
3.2	DETERMINATION OF SPECIFIC HEAT, C_p	73
3.3	DETERMINATION OF THERMAL CONDUCTIVITY	74
3.4	DETERMINATION OF COEFFICIENT OF LINEAR THERMAL EXPANSION, CTE.....	75
3.5	DECOMPOSITION TEMPERATURE	76
3.6	DETERMINATION OF GLASS TRANSITION TEMPERATURE	77
3.7	DETERMINATION OF MASTER CURVE BY RHEOMETER	78
3.7.1	DETERMINATION OF EXPERIMENTAL CONDITIONS FOR RHEOMETER TESTS	78
3.7.2	ARRHENIUS RELATION FOR RHEOMETER DATA	85
3.7.3	TIME – TEMPERATURE SUPERPOSITION (TTS) VALIDITY ..	89
3.7.4	REFERENCE TEMPERATURE SELECTION	91
3.8	DETERMINATION OF MASTER CURVE BY MECHANICAL TESTS .	91

3.8.1 DETERMINATION OF EXPERIMENTAL CONDITIONS FOR MECHANICAL TESTS.....	91
3.9 MECHANICAL TEST RESULTS	92
3.9.1 ARRHENIUS RELATION FOR MECHANICAL TEST DATA	98
3.10 COMPARISON OF MASTER CURVES AND SHIFT FACTORS.....	101
CHAPTER 4 CONCLUSION.....	105
REFERENCES.....	107

LIST OF TABLES

TABLES

Table 1	Ingredients used in composite propellants (Davenas A., 1993 – 4).....	10
Table 2	Test conditions for glass transition temperature (T_g)	64
Table 3	Test conditions for rheometer.....	66
Table 4	Stress Relaxation Test Conditions.....	69
Table 5	Experimental shift Factors by rheometer	81
Table 6	Shift Factors calculated by WLF equation for rheometer	83
Table 7	WLF constants according to performed test conditions	83
Table 8	Representation of shift factors by WLF equation	85
Table 9	Representation of shift factors by Arrhenius equation.....	87
Table 10	Comparison of experimental, WLF and Arrhenius shift factors	89
Table 11	Test Conditions for Mechanical Tests.....	92
Table 12	Experimental shift factors calculated from mechanical tests	94
Table 13	Shift factors calculated by WLF equation for mechanical test results	96
Table 14	Representation of shift factors by WLF equation	98
Table 15	Representation of shift factors by Arrhenius equation.....	99
Table 16	Comparison shift factors for mechanical testing.....	101
Table 17	Comparison of shift factor calculated from each method	104

LIST OF FIGURES

FIGURES

Figure 1	Ingredients of a composite propellant	4
Figure 2	General mixing principle of propellant	9
Figure 3	Propellant Characterization	11
Figure 4	TMA Design.....	16
Figure 5	TMA probe configurations.....	17
Figure 6	TA Instruments Q 500 design	18
Figure 7	Block Diagram of Thermal Diffusivity Measurements.....	19
Figure 8	Maxwell Model	23
Figure 9	Voight – Kelvin Model	24
Figure 10	Generalized Maxwell and Kelvin models	25
Figure 11	Relation between moduli.....	26
Figure 12	Phase angle.....	28
Figure 13	Tension (left) and shear (right) modes of deformation (Merlette N., and Pagnacco E., 2012).....	29
Figure 14	Rheometer geometries (Concentric cylinder, cone and plate, parallel plate and torsion rectangular).....	31
Figure 15	DMA Design	32
Figure 16	Clamping configurations for DMA (3 point-bending, dual/single cantilever, compression, shear sandwich and tension).....	33
Figure 17	Illustration of stress relaxation curves at different temperatures T_1 , T_2 and T_3	34
Figure 18	Individual modulus versus time graphs at different frequencies (Lake, 1999).....	36
Figure 19	Shifting along x – axis.....	37
Figure 20	Illustration of the shift factor.....	39
Figure 21	Invalid illustration of TTS with phase angle versus complex modulus plot (Gurp M., and Palmen J., 1998)	40

Figure 22	Valid illustration of TTS with phase angle versus complex modulus plot (Gurp M., and Palmen J., 1998)	40
Figure 23	Limiting value of the LVR range	42
Figure 24	Example of stress relaxation curves obtained at different temperatures (Yilmaz O., 2012).....	43
Figure 25	Examples of shifted stress – relaxation curves according to WLF equation (Yilmaz O., 2012).....	44
Figure 26	Removal of the propellant from its box.....	53
Figure 27	Slicing the propellant with guillotine	54
Figure 28	Propellant slices.....	54
Figure 29	Standard DSC Cell	55
Figure 30	LNCS Cooling System for DSC.....	57
Figure 31	Hermetically sealing of the sample pan	57
Figure 32	TA Instruments DSC Q200	58
Figure 33	TA Instruments Thermal Conductivity	60
Figure 34	Rheometric Scientific TMA 500	62
Figure 35	TA Instruments TGA Q 500.....	63
Figure 36	Instron 4481 50kN Tensile Testing System	67
Figure 37	Specimen Configuration.....	68
Figure 38	Dog bone samples for stress relaxation tests.....	69
Figure 39	Autoignition thermogram for the given propellant	72
Figure 40	Heat capacity of the given propellant within the temperature range of -60°C to 80°C	73
Figure 41	The voltage versus time graph for calculation of thermal conductivity..	74
Figure 42	CTE of the given propellant between -40°C to 100°C.....	75
Figure 43	Decomposition temperature of the given propellant	76
Figure 44	A typical dynamic mechanical test result for the propellant	77
Figure 45	Amplitude comparison at 0.2%, 0.5%, 1% and 2% strain at 20° at different frequencies.....	78
Figure 46	Complex modulus versus frequency data for rheometer results	80
Figure 47	Experimental shift factor calculation	80

Figure 48	Linearized WLF equation for rheometer shift factors.....	82
Figure 49	Master curve obtained with experimental shift factors (Table 5)	84
Figure 50	Master curve obtained with WLF shift factors (Table 6).....	84
Figure 51	$\ln a_T$ versus $1/T - 1/T_0$ plot for calculation of the activation energy .	86
Figure 52	Master curve obtained with shift factors calculated by Arrhenius relation	88
Figure 53	Illustration of Van Gorp Palmen plot (Gorp M., and Palmen J., 1998)..	90
Figure 54	Van Gorp Palmen plot for rheometer data (Phase angle versus complex modulus).....	90
Figure 55	A typical stress relaxation curve obtained at -20°C.....	93
Figure 56	Stress relaxation curves at different temperatures.....	93
Figure 57	Linearized WLF equation for mechanical shift factors.....	95
Figure 58	Master curve generated by using experimental shift factors.....	96
Figure 59	Master curve generated by using WLF shift factors	97
Figure 60	$\ln a_T$ versus $1/T - 1/T_0$ plot for calculation of the activation energy ..	99
Figure 61	Master curve generated with Arrhenius Shift Factors for mechanical test results	100
Figure 62	Master Curve obtained with rheometer (Complex shear modulus E^* vs reduced time).....	102
Figure 63	Master Curve obtained with mechanical tests (Relaxation modulus E vs reduced time).....	103
Figure 64	Comparison of master curves obtained both with rheometer and mechanical tests.....	103

LIST OF ABBREVIATIONS

H	: Viscosity
F	: Force
γ, ϵ	: Strain
$\dot{\gamma}$: Shear Rate
δ	: Phase angle
σ	: Stress
τ	: Shear Stress
DMA	: Dynamic Mechanical Analyzer
G'	: Storage Modulus
G''	: Loss Modulus
T	: Time
t_r	: Reduced time
G^*	: Complex Modulus
T_g	: Glass Transition Temperature
T_m	: Melting Point
T_b	: Boiling Point
AP	: Ammonium Perchlorate
CTE	: Coefficient of Thermal Expansion
TTS	: Time Temperature Superposition
WLF	: Williams – Landel – Ferry Shift Function

a_T	:	Shift Factor
C_1	:	WLF equation constant
C_2	:	WLF equation constant
E_a	:	Activation Energy
E	:	Relaxation Modulus
E_∞	:	Equilibrium Modulus
DSC	:	Differential Scanning Calorimetry
TGA	:	Thermo gravimetric Analyzer
TMA	:	Thermo mechanical Analyzer
R	:	Ideal gas constant
A	:	Arrhenius equation constant
K	:	Rate constant
Pa	:	Pascal
λ	:	Thermal conductivity
α	:	Thermal diffusivity
P	:	Density
JANNAF	:	Joint – Army – Navy – NASA – Air Force
DOA	:	DioctylAdipate
STANAG	:	Standardization Agreement
LVR	:	Linear viscoelastic Region
LNCS	:	Liquid Nitrogen Cooling System
NLVE	:	Non – Linear viscoelastic Region
NATO	:	North Atlantic Treaty Organization

ASTM	:	American Society for Testing and Materials
HTPB	:	Hydroxyl terminated poly butadiene
T _{reference}	:	Reference temperature
MAPO	:	Tris {1-(2-methyl) aziridiny} phosphine oxide
IPDI	:	Isophoronediiisocyanate
HMX	:	Cyclotetramethylenetetranitramine
TDI	:	Toluene-2,4-diisocyanate
BHT	:	2,6 – di(tert – butyl) hydroxytoluene
RDX	:	Cyclotrimethylenetrinitramine
DDI	:	Dymerildiisocyanate
TEA	:	Triethanolamine
RSS	:	Residual sum of squares

CHAPTER 1

INTRODUCTION

Propellant and rocket studies have always attracted the attention due to its critical role in military field in maintaining the national security of countries. The first known rocket propellant is black powder which is a combination of Sulphur (fuel), potassium nitrate (oxidizer) and coal (fuel). In the 13th century, the black powder was first applied to fireworks and fire arrows (Benson, 2014). This combination was used in primitive rockets. However this first propellant was used in powder form which resulted in limited burning time, explosion risk and low efficiency. It was concluded that, the propellant should be homogeneous at micro level. In 19th century, industry was developing and scientists were offering new products. In late 1938, W. Parson mixed asphalt and potassium perchlorate (oxidizer) with black powder (fuel). This was the first composite propellant. In this case the problem was the danger in use of potassium perchlorate. In addition, in that period of time, nitrocellulose and nitroglycerine were discovered and they were used in propellant industry. In the second half of 20th century the first modern powders composed of aluminum and ammonium perchlorate were emerged.

Moreover, ballistic and plastic developments affected the propellant history during World War II. In 1950, the polyurethane chemistry has begun to develop. This progress led to high – energy products and created the composite double base propellants.

In addition to these, development of propellants was affected by insulation technologies. Thermal protection of structures, combustion control, and case-

propellant bonding issues required the action of this complementary field (Davenas A., 1993-1).

1.1 PROPELLANT CLASSIFICATION

1.1.1 LIQUID PROPELLANTS

Liquid propellants are divided into two groups: monopropellant and bipropellant. In monopropellant oxidizer and fuel are stored in the same tank. Unlike monopropellants, in bipropellants oxidizer and fuel are stored in separate tanks. Liquid propellants attract less attention than solid propellants due to their volumetric disadvantages and expensive process ability

1.1.2 SOLID PROPELLANTS

1.1.2.1 DOUBLE BASE – HOMOGENEOUS PROPELLANTS

Double base propellants are classified according to the base material it contains. Single based propellants contain nitrocellulose as an energetic additive. Double based propellants include nitroglycerine besides nitrocellulose. Nitrocellulose is dissolved in nitroglycerine to form gel. According to the production technique, double base propellants are divided into following subgroups:

- a) Extruded Double Base: In this type of propellant nitroglycerine and nitrocellulose are mixed in water and with the addition of some additives final product is obtained by extrusion.

- b) Cast Double Base: This type of propellant is obtained by casting of nitroglycerine and casting solvent on to a mould containing nitrocellulose and some additives (casting powder). The casting solvent swells and dissolves the nitrocellulose at an appropriate temperature.
- c) Composite Modified Cast Double Base: This type of propellant is obtained by addition of nitroglycerine and energetic additives to casting powder used in cast double base type propellants.
- d) Elastomeric Modified Cast Double Base: This type of propellant is obtained by addition of hydroxyl polymer or isocyanate cross linker to the casting solvent used in cast double base propellants.
- e) Cross Linked Double Base: This type of propellant is obtained by plasticization of binder in liquid nitric ester and nitramine mixture (Davenas A., 1993).

1.1.2.2 COMPOSITE – NON HOMOGENEOUS PROPELLANTS

Composite propellants are obtained by mixing a solid powder oxidizer and metal powder as fuel in a polymeric matrix. They are composed of a polymer backbone, ammonium perchlorate (AP) as an oxidizer and aluminum. Ammonium perchlorate (AP) is easy to obtain, can be milled to a range of particle sizes to facilitate burning rate control and is chemically stable. The main disadvantage of ammonium perchlorate usage is the presence of large amounts of hydrogen chloride in the combustion products. In certain atmospheric conditions it forms dense smoke and is corrosive in nature. The cyclic nitramine HMX (cyclotetramethylenetetranitramine) is sometimes used to replace a portion of the ammonium perchlorate to reduce the chlorine content in the exhaust. The humidity is absorbed by AP based composite

propellants if it is not isolated properly and it may cause AP – binder network to collapse (AGARD, 1997).

The polymer backbone is mostly polybutadiene. The 85– 90% of the propellant formed of granular solids. Additionally composite propellant can include crosslinking chemicals (MAPO, isocyanates (TDI, IPDI and polyols)), burning rate catalysts (ferrocene, copper chromate, etc.), curing agents and variety of processing ingredients (AP, Aluminum and HMX) (Kumari A., et al., 2013).

The propellant should perform hot gases which expand in the nozzle and create thrust. In addition, it should include an oxidizer – fuel which enables the burning of the grain by evolving the sufficient energy. The oxidizer and fuel ingredients are solid powders and they should give cohesion and homogeneity by incorporated into the binder (Davenas A., 1993-2).

In this study, a composite type non - homogeneous propellant was studied.

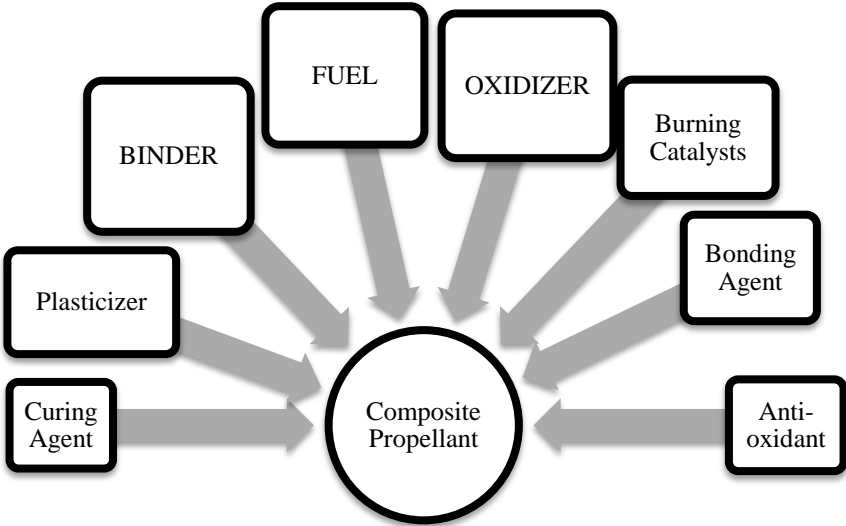


Figure 1 Ingredients of a composite propellant

1.2 INGREDIENTS OF A COMPOSITE PROPELLANT

The ingredients of a propellant can be classified in two groups: main additives and other additives. The main components of a propellant are binder, oxidizer and fuel. It can additionally contain other additives to improve mechanical and rheological properties.

1.2.1 MAIN ADDITIVES

1.2.1.1 BINDER

The binder is the backbone of the propellant. It should govern sufficient strength to avoid mechanical failure during storage or combustion. Binder should supply reactivity to propellant and provide additional fuel. Main component of binders are prepolymers. It is composed of a liquid prepolymer which is capable of crosslinking to provide dimensional stability to the product after crosslinking. Prepolymer is a repeating system of a monomer ending with a reactive functional group. Enthalpy of formation, oxygen content, glass transition temperature and average molecular weight affect binder's properties. Cross – linked systems have better mechanical properties compared to gel network systems. Degradation or failure may occur upon long term storage or environmental conditions (Sarner F., 1966). Hydroxyl-terminated polybutadiene (HTPB) is the most commonly used binder material. It enables a high solid fraction (88% to 90% of AP and Al by mass) and provides relatively good physical properties (Sutton G. P., and Biblarz O., 2010).

1.2.1.2 OXIDIZER

Oxidizer is the oxygen supply of the propellant mixture. An oxidizer should combine with fuel elements to release maximum possible energy and it should be compatible with fuel. The particle size and shape determine the amount that will be used in the binder. Ammonium perchlorate (AP) is the universal oxidizer used in composite propellants due to its high oxygen balance and relative stability. However, it produces hydrochloric acid upon combustion and it is toxic. In addition, RDX and HMX are used as oxidizers for some solid propellants even though they were developed as explosive ingredients to lower toxicity, thermal stability and lack of hydrochloric acid upon combustion (Sarner F., 1966).

1.2.1.3 FUEL

The fuel is a reducing agent and it should form high energy and low molecular weight products when it is oxidized. Aluminum is the universal fuel for the composite propellants and it is suitable for high solid loading. It can form flammable and explosive mixtures with air in powder form. Magnesium, lithium and boron can be used as fuel in some applications (Sarner F., 1966).

The major propellant properties, such as burning rate, rheology, and mechanical behavior, are directly depend on distribution of fuel and oxidizer particles and the size of the solid particles used in the composite propellant matrix.

1.2.2 OTHER ADDITIVES

1.2.2.1 PLASTICIZER

The plasticizers are non - reactive esters and hydrocarbons which have relatively low molecular weight and they should be compatible with binder. Plasticizers improve the processability of the propellant mixture and mechanical properties of a curing propellant. They affect mechanical properties by lowering T_g and modulus of the binder. Most commonly used plasticizers are DOA, IDP and DOP (Muthiah R., et al., 1989)

1.2.2.2 CURING AGENT

Crosslinking systems are polyfunctional molecules with low molar weight and provide chain length extension of prepolymers. They bind to prepolymer molecules and play critical role in mechanical strength of propellant. There are three types of polyaddition reaction: Addition of alcohol to isocyanate, addition of organic acid to an epoxide and addition of organic acid to an aziridine. Most commonly used curing agents are MAPO, IPDI, DDI and TDI (Rodic V., et al., 2005)

1.2.2.3 BONDING AGENT

The bonding agents are class of isocyanurates which enables interaction between the solid filler and the binder. They form an interaction between the oxidizer and binder by forming primary or secondary bonds. Bonding agents enables decrease in surface energy of solid additives and provide better wetting of the surface by the binder. Most commonly used bonding agents are MAPO and TEA (Petkovic J., et al., 2009).

1.2.2.4 BURNING RATE MODIFIERS

Burning rate of the propellant is important for rocket motors. It depends on pressure, initial propellant temperature, velocity, propellant type, oxidizer – fuel ratio and oxidizer particle ratio. As a result it must be regulated with burning rate catalysts to enable the desired ballistic properties. The burning rate modifiers lower the decomposition temperature of AP or accelerate the decomposition of AP. The amount of these substances should be adjusted carefully since they are lowering energy and reduces the energy. There are also burning rate moderators which lowers the burning rate. Most commonly used modifiers are organic – metallic by products of copper, iron, chromium and boron (Bozic V., 2010).

1.2.2.5 ANTI – OXIDANTS

The binder, HTPB used in composite propellants, has terminal and reactive hydroxyl groups. These groups in a propellant mix react with diisocyanate to form polyurethane backbone. This backbone then plays a role in binding the solid particles in the propellant mix. However due to its repeating character, it may contain unsaturated units which are prone to oxidation. This oxidation process leads to aging of the propellant and changes mechanical properties. To overcome this problem, the anti – oxidants are added to the propellant mix. These additives prevent the oxidation of binder and provide longer safe storage time for propellant (Villar L. D., et al., 2010).

All the ingredients given above are mixed according to Figure 2 (Davenas A., 1993-3).

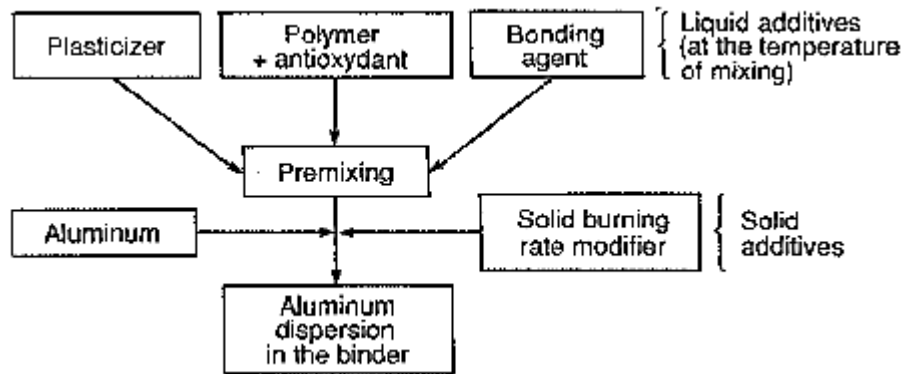


Figure 2 General mixing principle of propellant

1.3 PROPELLANT CHARACTERIZATION

The characterization of a propellant is very difficult when its response under loading conditions (direction, magnitude and speed) is considered. In recent years a working group of Sub Group 1 of NATO AC 310 has made a documentation of explosive materials which includes solid propellants. For structural analysis of propellant following parameters should be determined: CTE, thermal conductivity, stress – strain relationship. In addition to these, decomposition temperature, auto ignition temperature, T_g , C_p and gel/cure time parameters are also important for quality and process control (AGARD, 1997).

In this study, characterization of a propellant was divided in three main groups: Thermally, rheologically and mechanically.

Table 1 Ingredients used in composite propellants (Davenas A., 1993 – 4)

<u>TYPE</u>	<u>ABBREVIATION</u>	<u>FULL NAME</u>
Oxidizer	AP	Ammonium perchlorate
	AN	Ammonium nitrate
	NP	Sodium perchlorate
	KP	Potassium perchlorate
	RDX	Cyclotrimethylenetrinitramine
	HMX	Cyclotetramethylenetetranitramine
Binder	PBAN	Polybutadiene acrylonitrile
	CTPB	Carboxyl terminated polybutadiene
	HTPB	Hydroxyl terminated polybutadiene
Curing / Cross – Linking agents	PQD	Paraquiononedioxime
	TDI	Toluene-2,4-diisocyanate
	MAPO	Tris {1-(2-methyl) aziridinyl} phosphine oxide
	IPDI	Isophoronediiisocyanate
Bonding Agent	MAPO	Tris {1-(2-methyl) aziridinyl} phosphine oxide
	TEA	Triethanolamine
	MT-4	Adduct of MAPO, Azipic Acid and tartaric acid
Plasticizer	DOA	Dioctyladipate
	IDP	Isodecylpelargonete
	DOP	Dioctylphthalate
Burning Rate Catalyst	Fe ₂ O ₃	Ferric oxide
	FeO (OH)	Hydrated – ferric oxide
	nBF	n – butyl ferrocene
	DnBF	di – n – butyl ferrocene
Metal Fuel	Al	Aluminum
Anti – oxidants	BHT	2,6 –di(tert – butyl) hydroxytoluene
	TEA	Triethanolamine

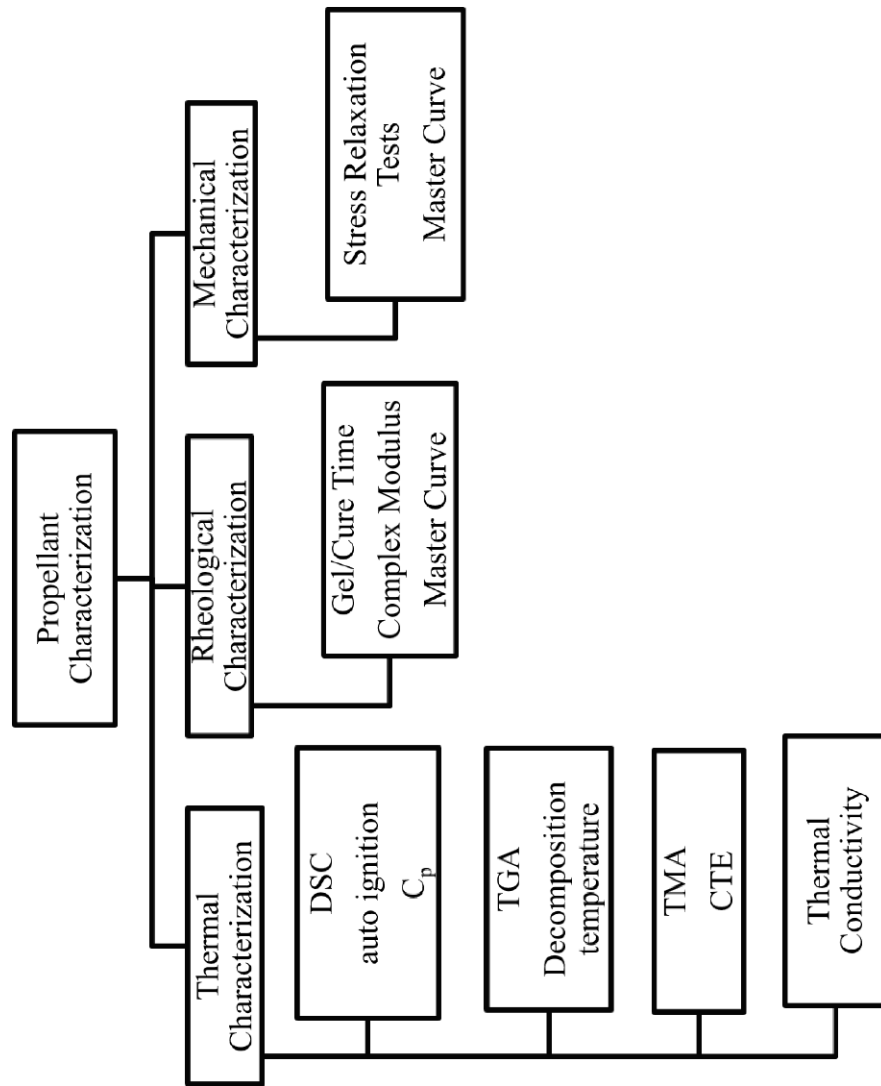


Figure 3 Propellant Characterization

1.4 CHARACTERIZATION CONCEPTS

1.4.1 THERMAL CHARACTERIZATION

1.4.1.1 AUTO IGNITION TEMPERATURE

It is defined as the minimum temperature at which a combustible material would ignite in air without the assistance of a spark or flame (Affens W. A., et al., 1974). It is important to determine the auto ignition temperature for safety of the rocket throughout its service life (Boggs W. H., 1976).

1.4.1.2 SPECIFIC HEAT, C_p

The specific heat capacity is the required amount of heat to raise the temperature of a substance by one degree (Krevelen D. V., 1972). Specific heat is an important physical property and it is used in calculation of specific impulse of a propellant which is a key parameter used to determine propellant performance since the burning rate depends on thermal diffusivity and thermal diffusivity is related to the specific heat (Santhosh G., et al., 2002).

1.4.1.3 COEFFICIENT OF LINEAR THERMAL EXPANSION, CTE

Linear thermal expansion is the change in length of a specimen due to a temperature change. The coefficient of linear thermal expansion $\alpha(T)$ is defined as the change in length per degree of temperature change divided by the initial length L_0 .

$$a(T) = dU/dT/L_0 \quad (1)$$

The initial length (L_0) is measured at a reference temperature (usually room temperature). a is expressed in units of inverse temperature (STANAG 4525 Ed1, 2001). CTE is an important parameter for material characterization and essential calculating the thermal stress in the rocket motor.

1.4.1.4 DECOMPOSITION TEMPERATURE

It is the temperature at which the weight change of the propellant occurs upon decomposition under temperature change. It determines the stability of the propellant (Rocco J. A. F. F. et al., 2004).

1.4.1.5 THERMAL CONDUCTIVITY

It is the property of the propellant to conduct heat (Ward J. R., 1977). It is important in burning characteristics of a propellant and it is required to carry out transient thermal stress analysis of rocket propellant grain.

Some techniques used for thermal characterization are DSC, TGA, TMA and thermal conductivity.

1.4.2 THERMAL CHARACTERIZATION METHODS

1.4.2.1 DIFFERENTIAL SCANNING CALORIMETRY (DSC)

DSC is a system that measures both the heat transfer and change in temperature of a sample with respect to a given, known standard reference material. The heat transfer is given as a function of time and temperature. The DSC system provides quantitative and qualitative data on endothermic (heat absorption) and exothermic (heat evolution) processes of materials during physical transitions such as phase changes, melting, oxidation, and decomposition. Typical measurements of DSC include:

- Glass transitions in amorphous/semi-crystalline materials
- Melting points and boiling points
- Crystallization time and temperature and percent crystallinity
- Heats of fusion and reactions
- Oxidative stability
- Purity
- Rate of cure and degree of cure
- Reaction kinetics
- Specific heat and heat capacity
- Thermal stability

Recently, DSC can be used in a modulated mode. Modulated DSC is used to study the same material properties as conventional DSC including: transition temperatures, melting and crystallization, and heat capacity. In addition to these, modulated DSC increase the amount of information that can be obtained from a single DSC experiment, thereby improving the quality of interpretation. In modulated DSC a more complex heating profile (temperature regime) is applied to the sample than is used in conventional DSC. Specifically, a sinusoidal modulation (oscillation) is

overlaid on the conventional linear heating or cooling ramp to yield a profile in which the average sample temperature changes sinusoidal rather than linearly (Sarner F., 1966).

Capabilities of Modulated DSC:

- Measurement of heat capacity and heat flow in a single experiment
- Separation of complex transitions into more easily interpreted components
- Increased sensitivity for detection of weak transitions
- Increased resolution of transitions without loss of sensitivity
- Increased accuracy in the measurement of polymer crystallinity

1.4.2.2 THERMO MECHANICAL ANALYZER (TMA)

TMA is a system which measures the dimensional change in the sample with respect to temperature under a certain load and controlled atmosphere.

The TMA uses interchangeable probes at varied loads to make a number of measurements. These measurements include:

- Softening temperatures or T_g
- Melting temperatures
- Stress relief effects at T_g
- Coefficients of thermal expansion (CTE)
- Dimensional compatibilities of two or more different materials
- Onset of foaming
- Relative degree of cure of thermosets
- Composite delamination temperatures
- Percent shrinkages of films and fibers
- Shrinkage forces

- Effectiveness of cling of films
- Testing of coatings on metals, films, optical fibers and electrical wires
- Assessment of transverse versus machine orientational properties of films

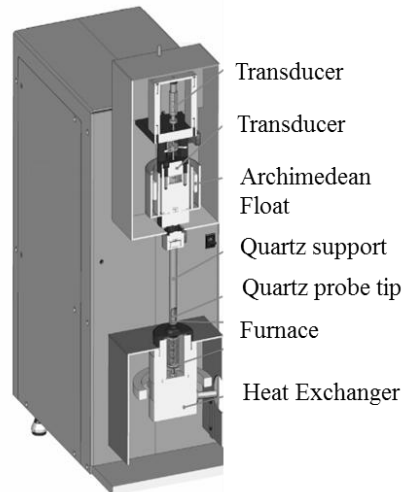


Figure 4 TMA Design

The most commonly used TMA probe is the expansion probe. This probe rests on the surface of the test specimen under low loading conditions. As the sample expands, during heating, the probe is pushed up and the resulting expansion of the sample is measured. By using this probe T_g and CTE can be calculated.

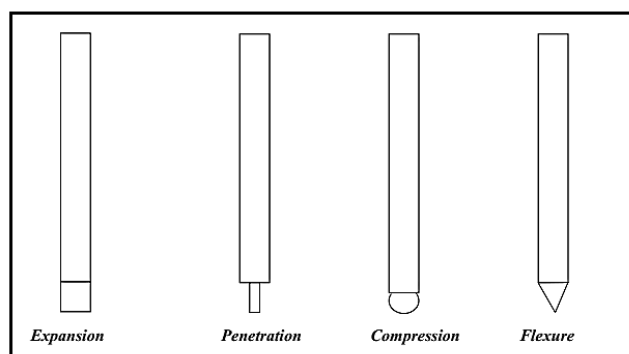


Figure 5 TMA probe configurations

The TMA penetration probe provides another means of assessing glass transition temperatures. When performing measurements with the penetration probe, loading is added to the probe so that it moves down through the material as it softens. The penetration probe is useful for measuring the glass transitions of coatings on a substrate. By using this probe T_g and softening point can be determined.

1.4.2.3 THERMOGRAVIMETRIC ANALYZER (TGA)

Thermogravimetric analysis (TGA) is a thermal analysis technique for measuring the amount and rate of change in sample mass as a function of temperature and time. It is used to characterize any material that exhibits weight loss or phase changes as a result of decomposition, dehydration, and oxidation. The general design of the instrument is given in Figure 6.

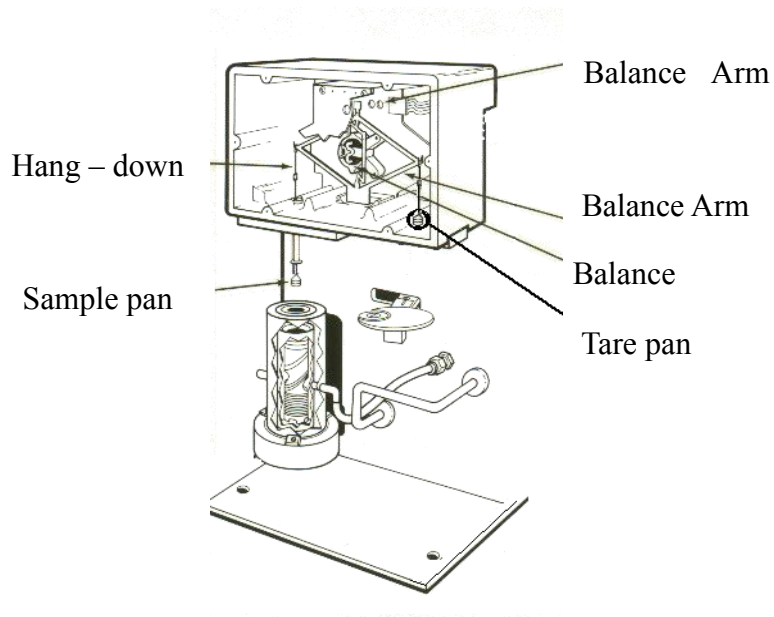


Figure 6 TA Instruments Q 500 design

1.4.2.4 THERMAL CONDUCTIVITY

Thermal conductivity is measured according to flash method indirectly. In this system, laser pulse sent on a sample disc and diffusivity measured. The energy of the pulse is absorbed on the front surface of the specimen and the temperature change in the back side of the specimen measured.

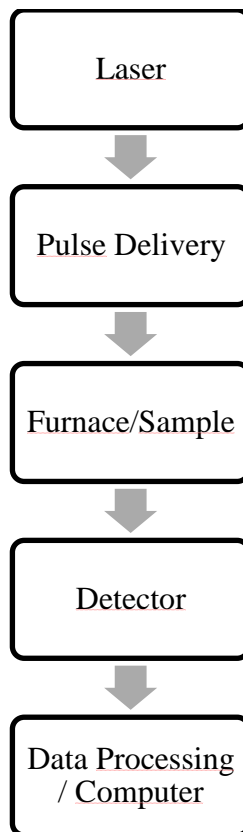


Figure 7 Block Diagram of Thermal Diffusivity Measurements

With thermal diffusivity results, by using density and specific heat, thermal conductivity is calculated with the help of Equation 2 (ASTM E1461 – 01).

$$\lambda = \alpha \times C_p \times \rho \quad (2)$$

λ : Thermal conductivity

α : Thermal diffusivity

C_p : Specific heat

ρ : Density

1.4.3 RHEOLOGICAL CHARACTERIZATION

1.4.3.1 RHEOLOGY

Rheology is a science of flow and deformation. Under an applied stress or strain rheology studies the response of a material (Tanjore D., 2005). Rheology is used to characterize an industrial process, to control quality of the product and to understand the behavior of materials.

1.4.3.2 TERMS AND CONCEPTS

When an external force (F) applied on a material, the material responds. The amount of applied force on the material per unit area (A) is called stress (σ). The stress is measured in the units of Pascal (Pa) (Tanjore D., 2005).

$$\sigma = \frac{F}{A} \quad (3)$$

Material's response under applied stress is called deformation. The resulting deformation is expressed in terms of strain (ϵ or γ). The deformation can also be defined as the flow of matter or change in dimension under a certain strain. Strain is called the ratio of elongation of specimen to original gauge length (STANAG 4507, Ed 1).

There are two kinds of stress classifications; normal stress and shear stress. If the applied force is perpendicular to the sample surface the stress is normal stress which results in normal strain. If the applied force is parallel to the surface, the stress is called shear stress and it results in shear strain (γ). Shear strain rate ($\dot{\gamma}$) or shear rate

is defined as the movement rate of layers of the material (Equation 4). It is expressed in s^{-1} (Tanjore D., 2005).

$$\dot{\gamma} = \frac{d\gamma}{dt} \quad (4)$$

A material is classified as elastic (ideal solids), viscous (ideal fluids) or viscoelastic according to its response under applied force. Ideal solids store energy during deformation under the applied force. When the force removed, ideal solids return to their original shape by using the stored energy. However in ideal fluids, they do not store but dissipate energy in the form of heat.

For ideal solids, Hooke's law given in Equation 5 is observed in which stress and strain are linearly related to each other where the slope, E is called the Young's modulus.

$$\sigma = E \times \epsilon \quad (5)$$

When the type of loading is shear, the relation is also valid as given in Equation 6.

$$\tau = G \times \gamma \quad (6)$$

On the other hand, for ideal fluids, Newton's law is given in Equation 7. The stress (τ) applied is proportional to strain rate and μ is the viscosity.

$$\tau = \mu \times \dot{\gamma} \quad (7)$$

A material which behaves between an ideal solid and an ideal liquid is called a viscoelastic material. A viscoelastic material shows an initial linear stress – strain relation at relatively sufficient small strain values (Bilyjk S., and Scheidler M. J., 2009). This behavior is called the linear viscoelastic behavior. Up to a certain point linear behavior continues; however after certain point material begins to show non –

linear viscoelastic behavior. Polymer melts, gels and dough can be examples of viscoelastic materials.

1.4.3.3 UNDERSTANDING VISCOELASTIC BEHAVIOR

To understand the viscoelastic behavior of materials simple mechanical models and their mathematical expressions are used. These models can be formulated by combining a number of springs and dashpots. The Maxwell model describes the stress relaxation behavior and Voight – Kelvin model describes the creep behavior. However, both models are inadequate to define the viscoelastic behavior individually. As a result, generalized models are used.

1.4.3.4 MAXWELL MODEL

This model is represented in Figure 8. The spring and the dashpot are connected in series. The model is used to simulate the behavior of viscoelastic liquids. The strain is equal to the summation of strain on the spring and the strain on the dashpot. Spring reflects the elastic behavior and dashpot represents the viscous behavior (Roylance D., 2005).



Figure 8 Maxwell Model

In this model elastic deformation is fast, instantaneous and viscous deformation is time dependent. When a constant strain is applied, by using this model, the change in stress with respect to time is computed. By this model stress relaxation behavior can be simulated.

1.4.3.5 VOIGHT – KELVIN MODEL

The model is based on a Voight element in which a spring and a dashpot are connected in parallel (Figure 9). Voight – Kelvin model simulates the viscoelastic material deformation under applied stress and material which restores its shape completely when the applied stress is removed (Fatseyu, 2005).

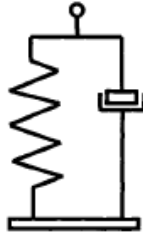


Figure 9 Voight – Kelvin Model

Under applied stress the spring will stretch to equilibrate and the dashpot will show damping resistance and it will delay elastic deformation. Viscoelastic deformations are explained with this model as given in Equation 8.

$$\sigma = E\gamma + \eta \frac{d\gamma}{dt} \quad (8)$$

Under the constant stress, ($d\sigma/dt = 0$) the equation becomes:

$$\gamma = \gamma_0 e^{\frac{-t}{\tau}} \quad (9)$$

Equation 9 can be used to simulate the creep behavior of the viscoelastic material. However with both models, the exact behavior of the polymer cannot be explained totally. Therefore, generalized Maxwell and Kelvin Models containing a number of relaxation times and retardation times are used to describe the behavior of polymer with many relaxation times.

1.4.3.6 GENERALIZED MODELS

Maxwell and Kelvin models are adequate for qualitative and conceptual analyses, but generally poor for the quantitative representation of the behavior of real materials. In order to improve the representation we need to increase the number of parameters by combining a number of springs and dashpots.

The generalized Maxwell model is composed of $n + 1$ constituent elements in parallel, being n Maxwell models and an isolated spring (Figure 10).

The generalized Kelvin model is composed of n Kelvin units in series plus an isolated spring (Marques and Creus, 2012).

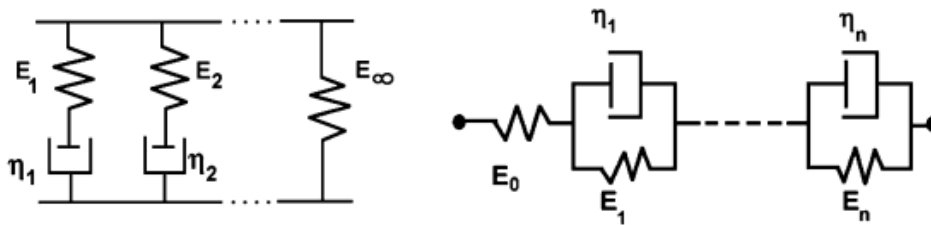


Figure 10 Generalized Maxwell and Kelvin models

1.4.4 RHEOLOGICAL CHARACTERIZATION PARAMETERS

1.4.4.1 MODULUS

Dynamic mechanical properties of the propellant can be expressed by three parameters; storage modulus, loss modulus and phase angle (loss factor).

- a) Complex Modulus, G^* : Complex modulus is the ratio of shear stress over shear strain determined in the linear viscoelastic region (Krevelend D. W., 1972).

$$G^* = G' + iG'' \quad (10)$$

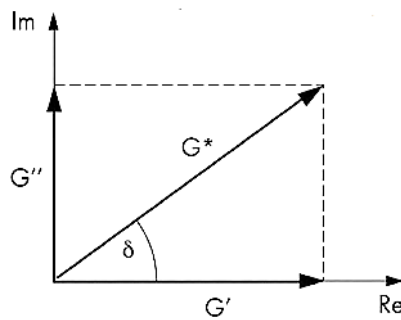


Figure 11 Relation between moduli

The magnitude of the complex modulus can be defined as in Equation 11:

$$G^* = \sqrt{G'^2 + G''^2} \quad (11)$$

- b) Storage Modulus, G' : It represents the energy stored within the material corresponds to elastic behavior. It is expressed as the product of complex modulus and the cosine of the phase angle:

$$G' = G^*(\cos\delta) = \frac{\tau}{\gamma}(\cos\delta) \quad (12)$$

- c) Loss Modulus, G'' : It is the measure of energy loss through dissipation and describes the viscous behavior.

$$G'' = G^*(\sin\delta) = \frac{\tau}{\gamma}(\sin\delta) \quad (13)$$

- d) Tan (δ), Phase Angle: It is the ratio of loss modulus to storage modulus. It can also be referred as the ratio of viscous effects over elastic effects.

$$\tan\delta = \left(\frac{G''}{G'}\right) \quad (14)$$

Stress is in phase with the strain for a perfectly elastic solid without any deviation. The phase angle is reported as 0° . On the other hand, the stress and strain are out of phase for a perfectly viscous liquid and the phase angle is reported as 90° (Tanjore D., 2005).

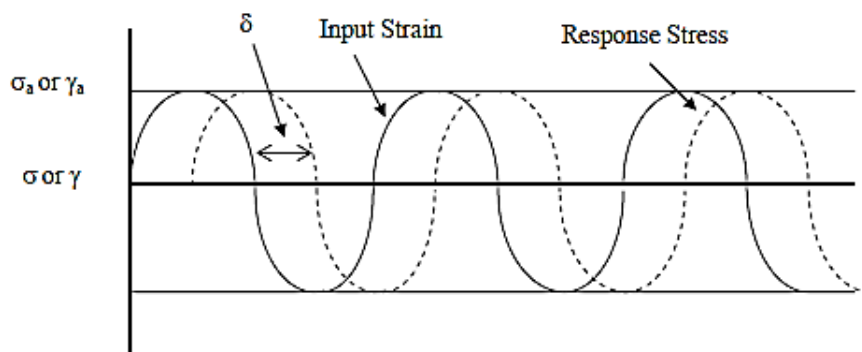


Figure 12 Phase angle

As a result for a material, If;

$G' > G''$, the material is more elastic,

$G'' > G'$ the material is more viscous.

In addition, if the phase angle of a material is in between 0° and 90° , the material is defined as viscoelastic (Tanjore D., 2005).

According to direction of applied force complex modulus can be represented in tensile mode as in Equation 15.

$$E^* = E' + iE'' \quad (15)$$

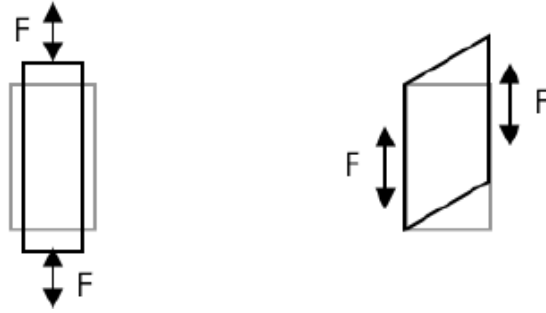


Figure 13 Tension (left) and shear (right) modes of deformation (Merlette N., and Pagnacco E., 2012)

There is a relation between Young's and shear moduli given in Equation 16.

$$G = \frac{E}{2(1+\nu)} \quad (16)$$

The definitions for moduli are valid in the linear viscoelastic region in which for a given strain rate material functions are independent of varying stress or strain. This enables the above equations applicable.

Viscoelastic properties like storage modulus, loss modulus, complex modulus and phase angle can be determined by rheometry or dynamic mechanical analysis (DMA).

1.4.4.2 GLASS TRANSITION TEMPERATURE, T_g

Since the propellant is a polymer based mixture, the behavior of the polymer is important. At low temperatures polymers are hard and brittle. They behave like glass. The thermal energy is lower than the potential energy barrier required for the polymer movement. The polymer chains behave like "frozen". Only vibrational

movements are observed. With increasing temperature, the vibrations increase and finally the thermal energy becomes sufficient and becomes enough to rotate the polymer molecule segments. This region is called the glass transition temperature (T_g) (Saçak M., 2002). It can be detected by monitoring the storage modulus and phase angle by DMA or rheometer and it can also be detected by DSC by monitoring the heat flow. The glass transition point is important for determination of lower operation temperature limit of the polymer based propellant. The change in T_g , during storage may be an indication of change in propellant behavior.

1.4.5 RHEOMETERS

Rheometry is the study of rheological parameters of a material. Rheometers are the instruments in which rheological properties are measured (Tanjore D., 2005). Rheometer can be divided into two groups: Rotational (Shear) rheometers and Extensional (Tensile/Bending) rheometers.

Rotational rheometer is capable of subjecting a sample to a dynamic (sinusoidal) or steady shear strain deformation, or the combination of dynamic and steady strain. Then the resultant torque generated by the sample, in response to this shear strain, is measured. Rotational rheometers are further divided into two sub groups: strain controlled and stress controlled rheometers.

Extensional rheometer is capable of applying extensional stress or strain on the sample. Extensional rheometers are less common due to problems associated with material properties.

Rheometers can perform flow, oscillation and transient tests and enable information about;

- Viscosity – function of shear rate or stress, time & temperature dependence

- Viscoelastic properties (G' , G'' , $\tan \delta$) with respect to time, temperature, frequency & stress/strain
- Glass transition temperature, T_g
- Transient response (relaxation modulus, creep compliance, creep recovery)

Rotational rheometers function with different geometries (Figure14);

- Concentric cylinder
- Cone and plate
- Parallel plate
- Torsion Rectangular

The choice of geometry depends on difficulty in loading, physical state of the material at the beginning and type of the test desired.

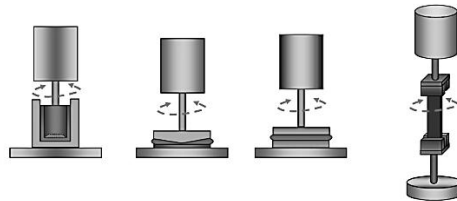


Figure 14 Rheometer geometries (Concentric cylinder, cone and plate, parallel plate and torsion rectangular)

1.4.6 DYNAMIC MECHANICAL ANALYZER (DMA)

Under an applied periodic stress, the DMA measures the properties of materials as they deform. A sinusoidal stress is applied to the material and resultant sinusoidal strain is measured (Menard K. P., 2008).

By this technique, fundamental material parameters, including storage and loss modulus, $\tan \delta$, complex and dynamic viscosity, storage and loss compliance, transition temperatures, creep, and stress relaxation, as well as rate and degree of cure, sound absorption and impact resistance, and morphology can be determined.

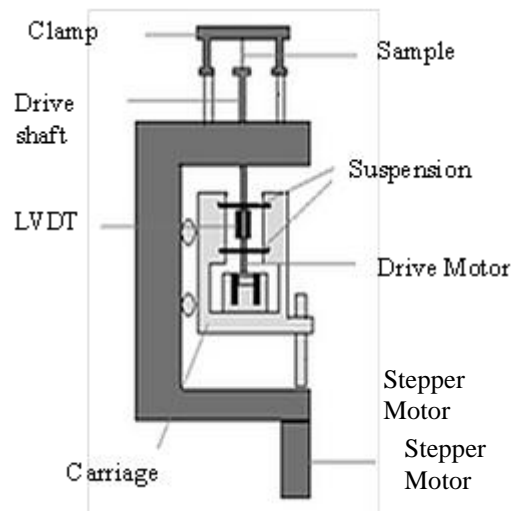


Figure 15 DMA Design

The DMA works with different sample geometries. The choice of geometry depends on difficulty in loading, physical state of the material at the beginning and type of the

test desired. The instrument provides 6 different clamping configurations (Figure 16):

- 3-point bending,
- Single cantilever / dual cantilever,
- Compression,
- Shear fixtures
- Tension

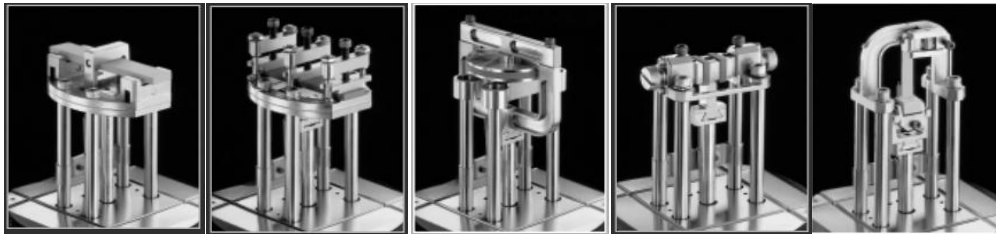


Figure 16 Clamping configurations for DMA (3 point-bending, dual/single cantilever, compression, shear sandwich and tension)

Most modern rheometers can function as a DMA instrument with DMA geometries up to a certain point defined by the manufacturer.

1.4.7 MECHANICAL CHARACTERIZATION

The mechanical properties of solid propellants are very important for proper functioning of the rocket. To be able to determine the mechanical properties stress – strain relation of propellant should be estimated. The material is exposed to a constant strain and stress is measured over time. Expected behavior is defined as the gradual decrease in stress. The illustration of a stress relaxation curve is given in Figure 17. Stress – relaxation tests are used further in stress analysis by deriving the master curve (Menard K. P., 2008).

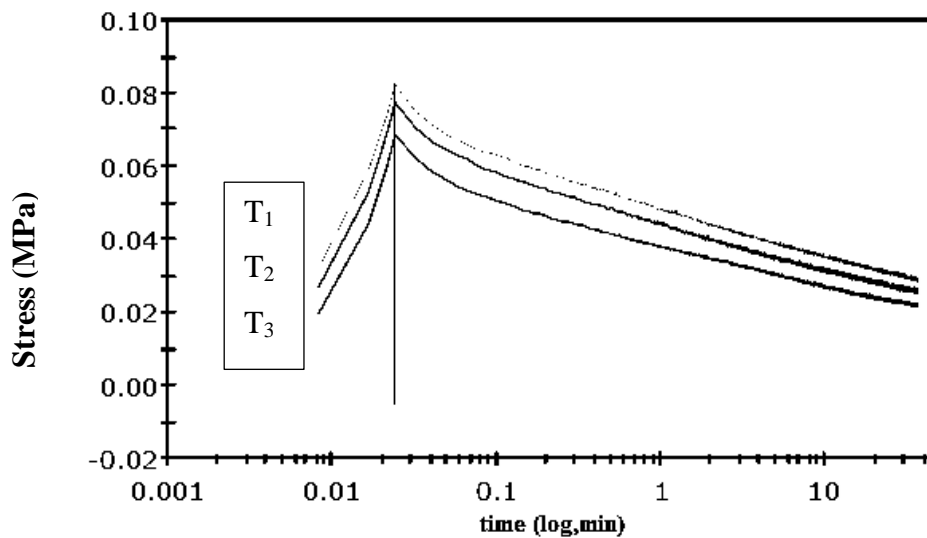


Figure 17 Illustration of stress relaxation curves at different temperatures T_1 , T_2 and T_3 .

The Young's modulus is measured as a function of time and called the relaxation modulus (Yılmaz O., 2012).

$$E(t) = \frac{\sigma(t)}{\gamma_0} \quad (17)$$

1.4.8 TIME – TEMPERATURE SUPERPOSITION AND MASTER CURVES

1.4.8.1 WHAT IS A MASTER CURVE?

Master curve is a single modulus versus time graph which is obtained by shifting overlapping individual modulus versus time graphs obtained by frequency sweep at different temperatures along the time axis. The curves are generated according to time – temperature superposition.

Master curves are used for quality control of the end product, long term stress/strain behavior of a material and they are important tools providing information about broader ranges of frequency or temperatures at which testing is not practical. Therefore with the help of master curves customer satisfaction is improved (Okubo N., 2009).

1.4.8.2 THE TIME – TEMPERATURE SUPERPOSITION:

It was observed that time and temperature has the same effect on viscoelastic materials. At low temperatures, material behaves as it is in high frequencies, at high temperatures; material behaves as it is in low frequencies.

At different temperatures and narrow frequency (time) ranges, it is possible to obtain individual modulus versus time graphs with frequency sweeps (Figure 18).

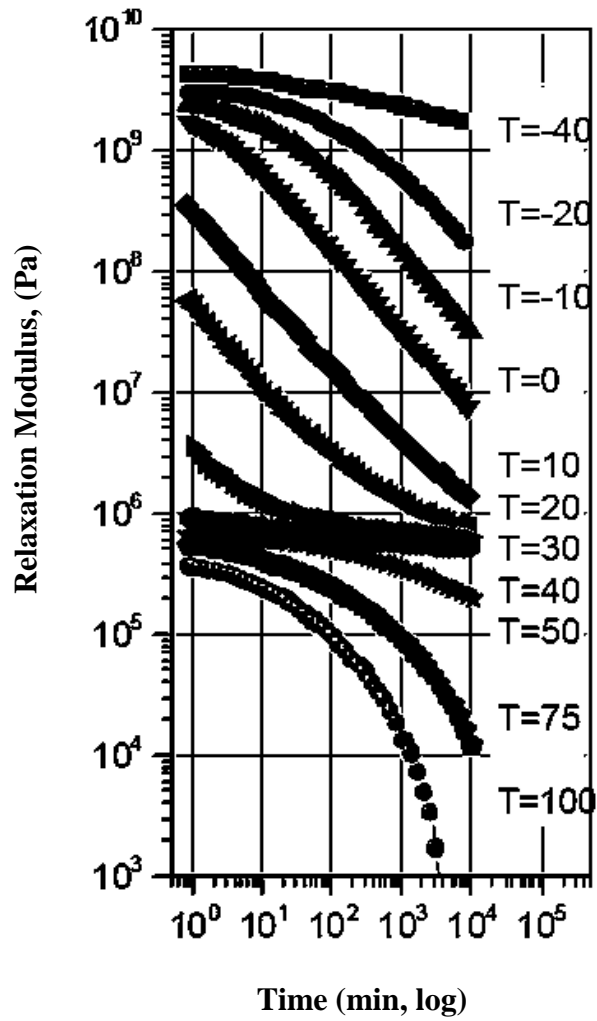


Figure 18 Individual modulus versus time graphs at different frequencies (Lake, 1999)

These individual curves can be shifted along the time axis according to the shift factors calculated.

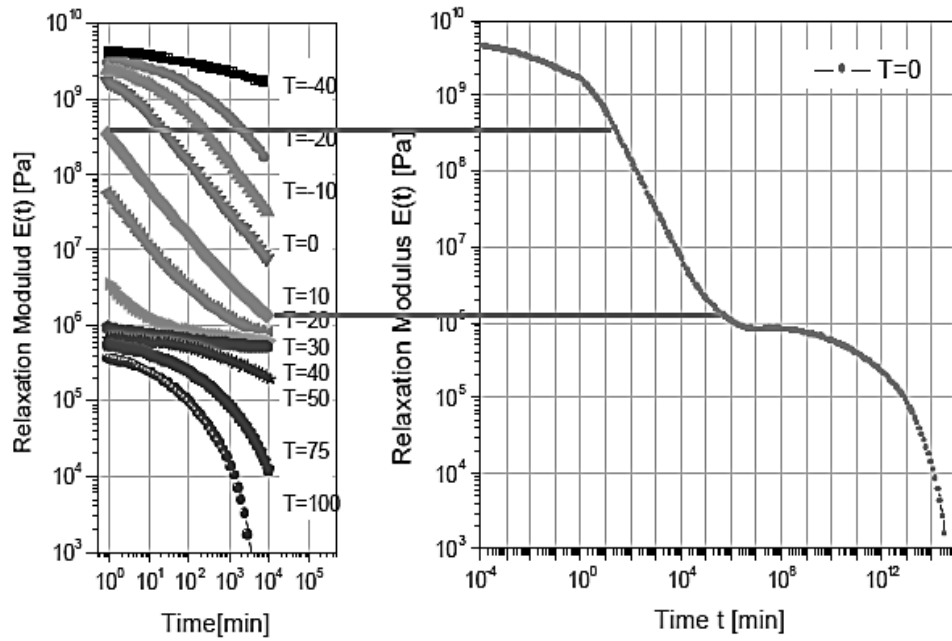


Figure 19 Shifting along x – axis

Shift factor determines the amount each reduced modulus has to be shifted along the logarithmic time axis in obtaining the master curve and they are determined by Williams – Landel – Ferry (WLF) equation (Equation 18). The shift factors are calculated according to a reference temperature. This reference temperature is generally equal to T_g of the material or room temperature (Krevelend D. W., 1972).

$$\log a_T = -C_1 \frac{(T-T_0)}{C_2+T-T_0} \quad (18)$$

Where;

C_1 and C_2 are empirical constants which depend on reference temperature and material

T is the temperature of interest

T_0 is the reference temperature

a_T is the shift factor

The constants C_1 and C_2 are material dependent parameters that have been associated with fractional free volume and the empirical Doolittle expression, and are defined as $B/2.303$ fg and fg/af, respectively. The values of $C_1=17.4$ and $C_2=51.6^\circ\text{K}$ were originally thought to be “universal” and are still widely used.

Generally in WLF equation, reference temperature is used as glass transition temperature of the material. For any other reference temperature selection, the generalized WLF equation (Equation 19) is used.

$$\log a_T = \frac{-A(T-T_{ref})}{B+(T-T_{ref})} \quad (19)$$

To be able to calculate the constants A and B, the linearized WLF equation was used. The Equation 19 is rearranged to derive Equation 20 (Billen J., 2012)

$$\frac{-(T-T_{ref})}{\log a_T} = \frac{B}{A} + \frac{1}{A}(T - T_{ref}) \quad (20)$$

Time – Temperature principle is valid for homogeneous, isotropic and amorphous materials. For any other material the applied time – temperature superposition should be checked for validity. Validity parameters are;

- No chemical or physical change at the selected temperatures
- Close temperature intervals to enable overlapping log curves of moduli
- Temperature intervals should be wide enough to enable sample relaxation in between temperature steps
- Linear plot of $\log a_T$ vs T
- Product of C_1 and C_2 should be independent of reference T selection
- Phase angle vs complex modulus curves

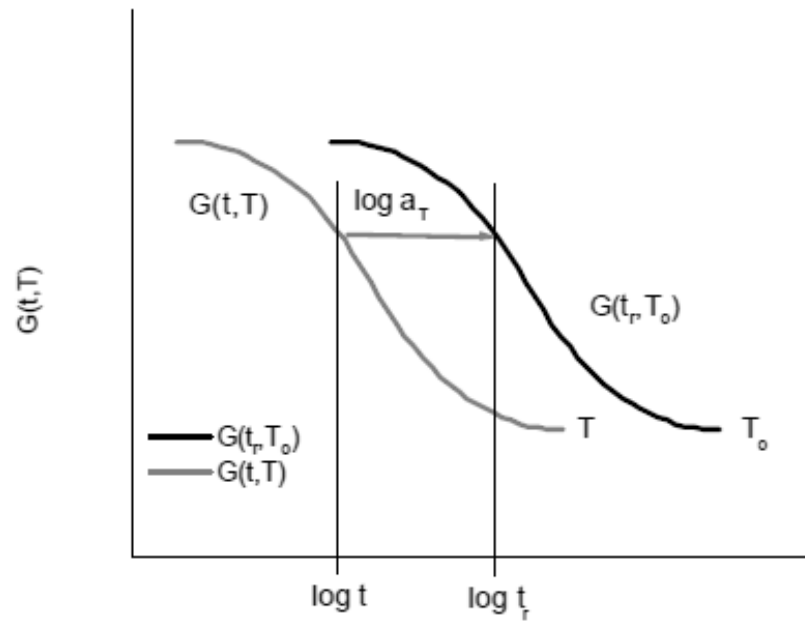


Figure 20 Illustration of the shift factor

1.4.8.3 TTS VALIDITY

During determination of master curves by rheometer, there are some important factors to be considered. Firstly, there should be no chemical or physical change during the measurement at the selected temperatures (Gurp M., and Palmen J., 1998). The temperature intervals should be selected close enough to enable overlap of logarithmic curves of moduli. Moreover the plot of $\log a_T$ versus temperature should give a smooth curve with no irregularities. The product of C_1 and C_2 constant should be independent of selection of reference temperature. The WLF equation should not be used when the selected temperature is 100°C above the T_g or below the T_g . In these conditions, it was concluded that Arrhenius relation works better.

In addition to these, phase angle versus complex modulus curves can be plotted. These plots eliminate the shifting effects along the frequency axis. Hence, it results in temperature independent curves when the TTS is valid (Hu M., 2011).

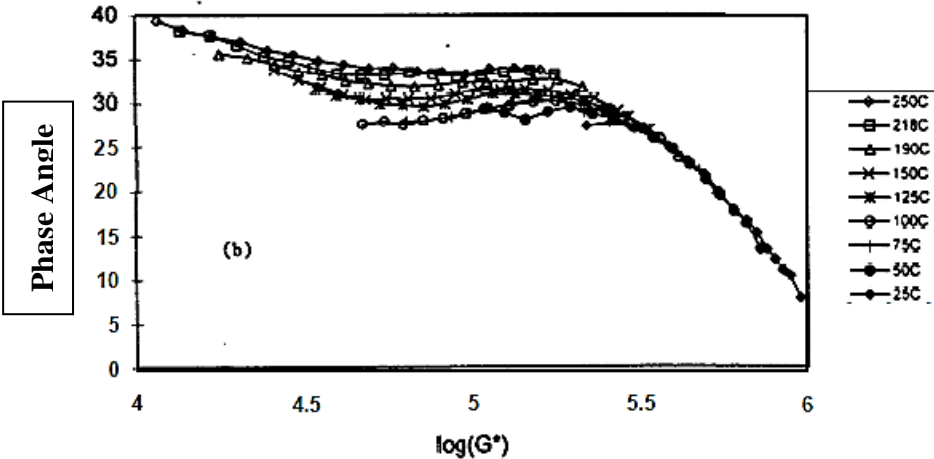


Figure 21 Invalid illustration of TTS with phase angle versus complex modulus plot (Gurp M., and Palmen J., 1998)

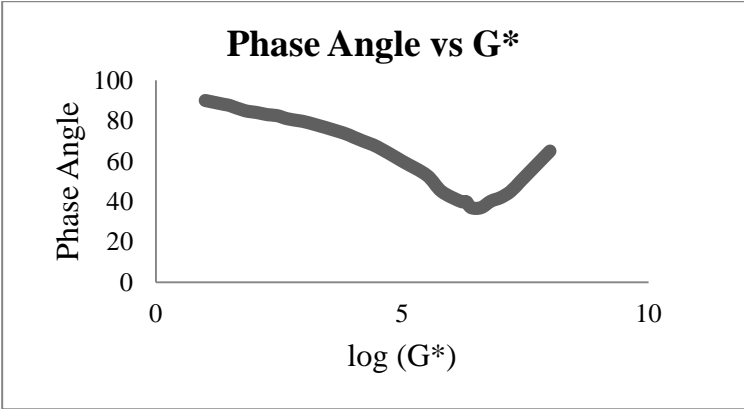


Figure 22 Valid illustration of TTS with phase angle versus complex modulus plot (Gurp M., and Palmen J., 1998)

1.4.8.4 ARRHENIUS RELATION AND ACTIVATION ENERGY

In 1899, Svante Arrhenius derived a relation by combining concepts of activation energy and Boltzman distribution law. This relation is called the Arrhenius Equation and it enables a connection between temperature and reaction rate. It can be derived from Equation 21 that, for high temperature and low activation energies, larger rate constants are calculated (Petrou A., et al., 2002)

$$k = A \times e^{\frac{-E_a}{RT}} \quad (21)$$

Besides master curve derivation, rheometer enables calculation of activation energy for the transition occurred in the temperature range of interest. The Arrhenius equation can be further rearranged to calculate the activation energy. By taking logarithm of the both sides in Equation 21, the Equation 22 can be derived.

$$\ln k = \frac{-E_a}{R \times T} + \ln A \quad (22)$$

In addition to this, the Arrhenius equation can be used to calculate the shift factors and with an analogy to Equation 22 the Equation 23 below can be built:

$$\ln a_T = \left(\frac{E_a}{R}\right) \times \left(\frac{1}{T} - \frac{1}{T_0}\right) \quad (23)$$

By using Equation 23, it is possible to plot $\ln a_T$ vs $\left(\frac{1}{T} - \frac{1}{T_0}\right)$ graph. The slope of the plot is $\frac{-E_a}{R}$. The activation energy can be calculated by using this equation.

Master Curves can be obtained by two techniques: Rheometry and mechanical testing.

1.4.8.5 DETERMINATION OF MASTER CURVE BY RHEOMETER

The linear viscoelastic region of the material is determined by strain sweep tests. According to Figure 23, viscoelastic region is up to γ_L .

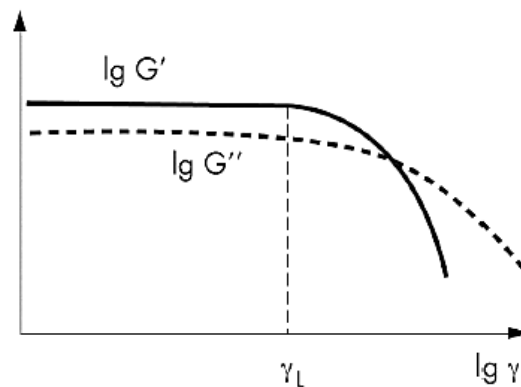


Figure 23 Limiting value of the LVR range

Then the material is subjected to different frequency ranges at different temperatures determined by the material's utility conditions. Storage modulus, loss modulus and complex modulus are obtained. The shift factors are calculated to shift the obtained curves by using WLF equation. The curves obtained are shifted according to the obtained shift factors according to a selected reference temperature.

Besides WLF equation, the Arrhenius equation given in 23 can be used to calculate the shift factors and the activation energy.

1.4.8.6 DETERMINATION OF MASTER CURVE BY MECHANICAL TESTING

Stress relaxation tests are used to determine the master curves by mechanical testing. The tests are carried out at different temperatures with a constant selected strain level and the stress values are measured. The relaxation modulus is obtained at the end of the tests. As temperature increases, modulus and stress of a viscoelastic material decrease as a function of time (Yilmaz O., 2012).

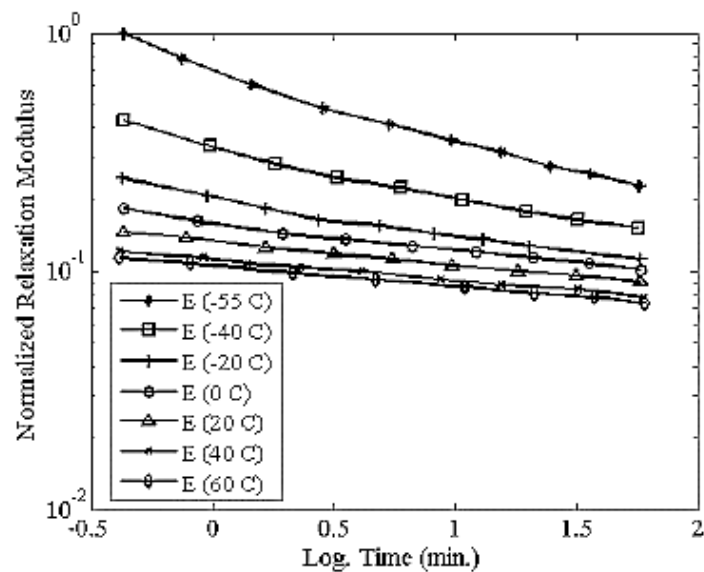


Figure 24 Example of stress relaxation curves obtained at different temperatures (Yilmaz O., 2012)

The shift factors are calculated using WLF equation to shift the obtained stress – relaxation curves according to a selected reference temperature.

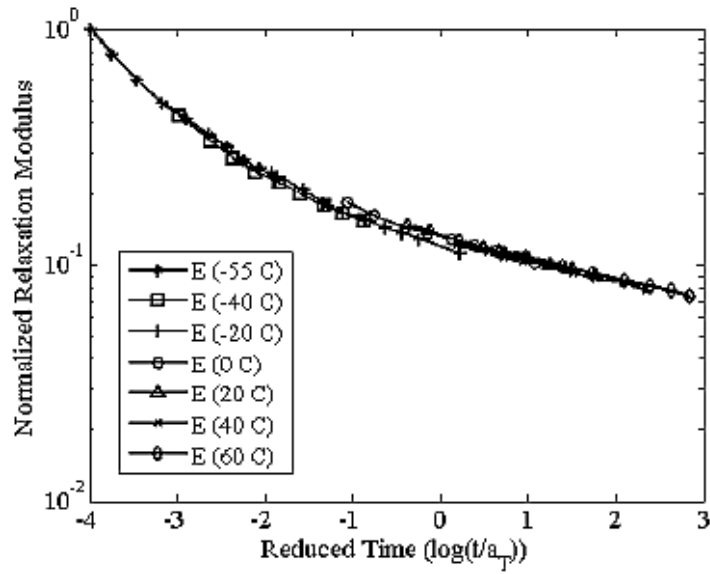


Figure 25 Examples of shifted stress – relaxation curves according to WLF equation (Yılmaz O., 2012)

When the obtained stress relaxation curves shifted along the horizontal axis the time is defined as the reduced time.

$$t_r = \frac{t}{a_T} \quad (24)$$

1.4.8.7 COMPARISON OF MASTER CURVES

To be able to compare the master curves obtained by both techniques, the types of deformations should be considered. In the mechanical testing, the Young's modulus is measured; however in rheometer the shear modulus is measured.

$$G^* = G' + iG'' \text{ (Complex shear modulus)} \quad (25)$$

For a truly isotropic material, the shear and the Young's modulus are related to each other by the Poisson's ratio, ν . It is 0.5 for incompressible materials.

$$G^* = \frac{E^*}{2(1+\nu)} \quad (26)$$

Then the equation becomes;

$$G^* = \frac{E^*}{3} \quad (27)$$

As a result, during the comparison of the master curves the moduli should be converted to each other.

In this study master curves will be obtained by both techniques: Rheometry and mechanical testing.

1.5 LITERATURE REVIEW

Many studies have been devoted to solid propellant and time temperature superposition studies. Landel, was first to investigate the viscoelastic properties of propellants (Landel F., 1961). Strahle released a final report on mechanisms on composite solid propellant combustion (Strahle W. C., et al., 1972). Buswell investigated the mechanical failure of composite propellants (Buswell J., 1975). A computer based approach for optimization of formulations was developed by Sakovich (Sakovich G. V., 1995). Kishore conducted a research on the effect of triethanolamine and benzaldehyde on storage stability of polystyrene – ammonium perchlorate propellant (Kishore K., et al., 1979). Components of a composite solid propellant were examined. Time – temperature Shift factors for gun propellants were

studied by Lieb and Leadore (Lieb R. J., and Leadore M. G., 1993). Asthana observed thermal behavior of AP – Based CMDB propellants with stabilizers. Master curves were obtained to calculate the shift factors over -40°C to 60°C (Asthana S. N., et al., 1992). Hunley summarized the history of solid rocket rocketry (Hunley J. D., 1999). Brostow studied prediction of temperature shift factor in longitudinal polymer crystal liquids. Master curves were obtained both by creep compliance measurements and stress relaxation tests (Brostow W., et al., 1999). Jeremic applied TTS for predicting mechanical properties of solid rocket propellants. Optimal test conditions like temperature and strain for determining the mechanical properties of rocket propellants for determination of master curves were investigated (Jeremic R., 1999). Herder compared the master curves obtained by DMA and mechanical testing for rocket propellants. Shift factors were calculated and at low temperatures differences were observed (Herder G., et al., 2003). Rowe and Sharrock, developed standard techniques for calculation of master curves for viscoelastic materials (Rowe G. M., and Sharrock M. J., 2000). Wingborg observed the enhancing effects of different isocyanates and chain extenders on HTPB (Wingborg N., 2002). Jain summarized the solid propellant binders (Jain S. R., 2002). Polacco studied dynamic master curves of asphalt mixture with 3 different geometries via DMA (Polacco G., et al., 2003). Wingborg did a research on improving mechanical properties of composite rocket propellants (Wingborg N., 2004). Witczak studied master curves for asphalt mixtures by dynamic mechanical analysis (Witczak M. W., 2004). Rodic and Petric observed the effect of additives on solid rocket propellant characteristics (Rodic V. and Petric M., 2004). Nevière conducted a research on extension of the time–temperature superposition principle to non-linear viscoelastic solids by DMA. Results obtained by tensile tests were shifted according to the shift factors calculated by DMA (Nevière R., 2006). Ronan, used time – temperature superposition for long term stress relaxation prediction of elastomers (Ronan S., et al., 2007). Cai, investigated the combustion in rocket environment. They used a combustion model to determine propellant behavior (Cai W., et al., 2008). Bilyk and Scheidler, studied the mechanical response and shear initiation of double based propellants by DMA (Bilyk S. R., and Scheidler M. J., 2009). Cerri conducted a research on ageing behavior of

HTPB based rocket propellant formulations (Cerri S., et al., 2009). In addition, Dealy, published an article about TTS for viscoelastic polymers and discussed the shift factors (Dealy J., 2009). Villar investigated the role of antioxidant on propellant binder activity during thermal aging (Villar L. D., et al., 2010). Kai developed a new method to obtain shear modulus of solid propellant (Kai D., et al., 2011). Mehilal, studied the storage life of propellants with different burning rates with DMA. Viscoelastic parameters of the propellant were determined and master curves were obtained for each kind of propellant (Mehilal et al., 2012). Merlette and Pagnacco, studied the dynamics of solid propellants with frequency dependent properties. The tension – compression and shear deformation were compared (Merlette N., and Pagnacco E., 2012). Mehilal studied the influence of testing parameters on dynamic and transient properties of solid propellant by DMA. They investigated the choice of parameters like temperature, frequency, strain level and stress level (Mehilal, et al., 2012). Mehilal studied the effect of experiment environment on calorimetric value of composite solid propellants (Mehilal et al., 2013). Zhang estimated the thermophysical properties of solid propellants based on particle packing model (Zhang J. W., et al., 2013). Mušanić studied the dynamic mechanical analysis of artificially aged double base rocket propellant (Mušanić S., et al., 2013). Gurp and Palmen studied TTS for polymeric blends and they investigated the validity of this superposition (Gurp M., and Palmen J., 1998). Chaturvedi and Dave published a review about solid propellants. The review summarizes the components and properties of propellants (Chaturvedi S. and Dave P. N., 2014). Kakumanu released a study about combustion study of composite solid propellants containing metal phthalocyanines (Kakumanu L. V., et al., 2014). Kakavas studied the mechanical properties of propellant composite materials reinforced with ammonium perchlorate particles (Kakavas P. A., 2014).

1.6 AIM OF THE STUDY

Determination of master curves for viscoelastic materials is important for characterization of the material. Conventionally, master curves are generated by mechanical tests. However, mechanical tests last for long test hours. To perform these tests, too much manpower is required. In addition, due to large number of testing sample is required for mechanical tests, the cost is very high.

On the other hand, master curves can be generated by rheometer. According to the temperature ramp rate and frequency range test duration may change. But the longest test lasts for 6 hours and with a single run result is achieved. Since torsion rectangular geometry is used, only a specimen with 12.5 mm width, 2-3mm thickness and 50 mm length is enough to estimate the master curve. Moreover, for data analysis, the instrument software is capable of directly deriving the master curve, activation energy and the shift factors in WLF equation. This eliminates errors may originate from data analysis carried out in mechanical test results.

In ROKETSAN, the propellant is manufactured by *explosives and propellant technologies department*. The tests are being done by *material characterization laboratory*. The data are analyzed by *structural analysis and test department*. It can easily be concluded that only for master curve derivation 3 separate departments are working which is not practical and time consuming. In addition to these, the data obtained by mechanical testing are analyzed manually with the help of regular computer programs. Since the process requires long working hours, it can only be conducted for selected propellant batch.

The aim of this study is to reduce the work load on different departments working under the roof of ROKETSAN, eliminate errors which may originate from calculations, reduce the amount of mechanical tests and sample amounts and obtain master curves practically by rheometer. According to the results concluded with this

study, master curves will be obtained for every single propellant batch manufactured in ROKETSAN. Furthermore, the goal is to get direct calculation of shift factors and activation energy hence to monitor propellant properties.

In order to achieve these goals, the study was planned as follows:

- Thermal characterization of the propellant will be completed in the first place.
- The propellant test samples will be tested at different strain values (0.2%, 0.5%, 1% and 2%) to be able to determine linear viscoelastic region.
- The master curve will be generated by rheometer.
- Shift factors will be calculated by rheometer test results.
- The activation energy will be calculated with rheometer test results.
- The stress – relaxation tests will be conducted for determination of the master curve by mechanical tests.
- Shift factors will be calculated by mechanical test results.
- The activation energy will be calculated with mechanical test results.
- The master curves, activation energies and shift factors obtained by two different techniques will be compared.

CHAPTER 2

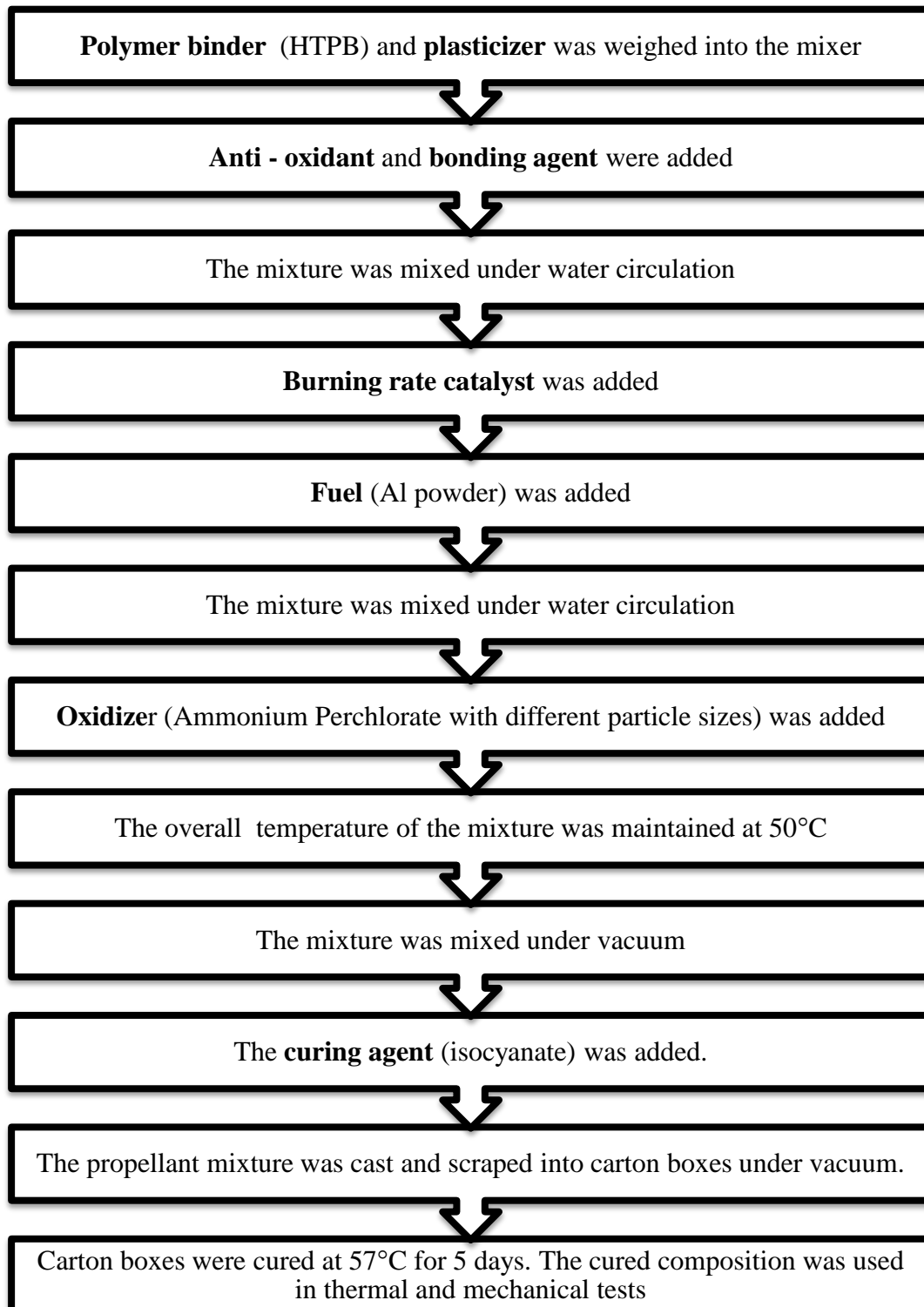
EXPERIMENTAL

2.1 CHEMICALS

The propellant mix was prepared with various chemicals both purchased from local or foreign suppliers. Some chemicals used in the propellant mix were obtained from different countries and manufacturers. The binder was supplied from Korean producer. The plasticizer was purchased from a local company in Turkey. Curing agent used in the propellant mix was supplied from a company, USA. Burning rate catalyst was again obtained from a producer from USA. The other ingredients; fuel, oxidizer, anti - oxidant and bonding agent are also obtained from local producers in Turkey.

2.2 PREPARATION OF THE PROPELLANT MIXTURE

The propellant mix was prepared in 300 gallon mixer. The mixer used in the mix has water circulation system to enable the desired temperature throughout the process. It has two stainless steel blades which accumulated closely each other for better dispersion of solid materials. The blades circulate in opposite directions with respect to each other to provide maximum swirling. Due to the explosive character of the propellant, the mixing process was initiated by remote control after each step. The temperature was kept at 50°C during the process and mixing durations were 30 minutes between each addition. The process parameters and amount of materials used in the propellant mix were determined by ROKETSAN. All the ingredients of the propellant were mixed according to the flow chart given in the following page.



2.3 PREPARATION OF PROPELLANT SAMPLES FOR TESTS

The propellant samples were prepared and put into carton boxes for curing. They were cured at 57°C for one week. After the cure, they were ready for sample preparation. The test samples were prepared stepwise as follows:

- a) The propellant was ripped out of this carton box (Figure 26).



Figure 26 Removal of the propellant from its box

- b) From the above part of this block propellant 3-4 cm was cut and separated to waste. From the remaining part of the propellant, with the help of guillotine, slices were cut (Figure 27).



Figure 27 Slicing the propellant with guillotine

- c) These slices were inspected for voids, cracks or any other physical defects.
The ones with defects were not tested.

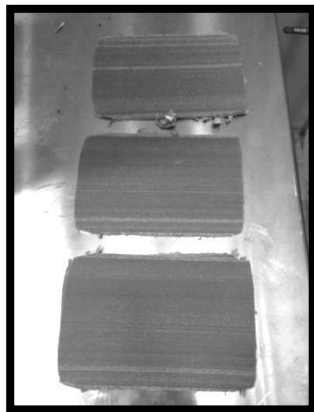


Figure 28 Propellant slices

The prepared test samples were wrapped into aluminum foil and stored in the desiccator until testing.

2.4 PROPELLANT CHARACTERIZATION

2.4.1 THERMAL CHARACTERIZATION

2.4.1.1 AUTOIGNITION TEMPERATURE

The autoignition of the chosen propellant was determined by TA Instruments DSC Q 200. The Q 200 DSC has a measuring cell with thermocouples integrated. The cell sensor consists of a constant body with separate raised platforms to hold the sample and reference. The platforms are connected to the heating block (base) by thin-walled tubes that create thermal resistances between the platforms and the base.



Figure 29 Standard DSC Cell

Thermocouples under each platform measure the temperature of the sample and reference. A third thermocouple measures the temperature at the base. The equation below shows the thermal network model which represents this cell arrangement, and the resultant heat flow expression that describes this cell arrangement.

$$q = -\frac{\Delta T}{R_r} + \Delta T_0 \left(\frac{R_r - R_s}{R_r R_s} \right) + (C_r - C_s) \frac{dT_s}{dt} - C_r \frac{d\Delta T}{dt} \quad (28)$$

R_r : Reference resistance

R_s : Sample resistance

C_r : Reference capacitance

C_s : Sample capacitance

T_r : Reference temperature

T_s : Sample temperature

The first term in this expression 28 is the equivalent of the conventional single – term DSC heat flow expression. The second and third terms account for differences between the sample and reference resistances and capacitances respectively. These terms have their largest impact during regions of the thermal curve where the heat capacity of the sample is the predominant contributor to heat flow. The fourth term accounts for the difference in heating rate between the sample and reference. This term has its largest impact during enthalpic events (e.g., melting).

For the cooling process, universal cooling accessory, The LNCS (Liquid Nitrogen Cooling System) was used. The Liquid Nitrogen Cooling System (LNCS) allows automatic and continuous temperature control within the range of 180°C to

550°C. The LNCS tank is pressurized to deliver the liquid nitrogen to the heat exchanger, which in turn cools the cell.



Figure 30 LNCS Cooling System for DSC

In this study, during auto ignition temperature determination, the sample pieces were used obtained from section 2.2. The 1.85 mg of propellant was accurately weighed into a hermetically sealed aluminum DSC pan.

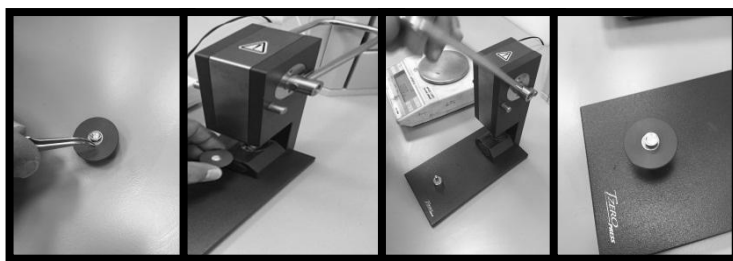


Figure 31 Hermetically sealing of the sample pan

The hermetic lid was punctured with a needle to enable gas evolution during decomposition. Another aluminum DSC pan was also hermetically sealed and used as a reference. The test was conducted according to STANAG 4515. The sample was heated from 25°C to 550°C with a heating rate of 10°C/min under nitrogen atmosphere. The sample purge flow was 50 mL/min. The results were reported in °C.



Figure 32 TA Instruments DSC Q200

2.4.1.2 SPECIFIC HEAT, C_p

The specific heat measurement was conducted by TA Instruments Q200 DSC in modulated (MDSC) mode. The C_p was calculated according to Equation 29.

$$C_p = (\beta \times A_{mhf} \times KC_p) \times (A_{mhf} \times W_s) \quad (29)$$

where:

β = Heating Rate

C_p = Specific heat capacity of the specimen, J/g °C,

A_{mhf} = Amplitude of the modulated heat flow, mW,

A_{mhr} = Amplitude of the modulated heating rate °C/min,

W_s = Mass of the sample mg, and

KC_p = Calibration constant

During specific heat determination, the sample pieces were used from section 2.3. 99.7 mg of propellant was weighed into a hermetically sealed aluminum DSC pan. The hermetic lid was punctured with a needle to enable gas evolution during decomposition. Another aluminum DSC pan was also hermetically sealed and used as a reference. The test was conducted according to ASTM E2716-09.

The sample was equilibrated at -100°C and modulated +/- 1°C for every 60 seconds. Then the sample was kept isothermally for 5 minutes. In the last step sample was heated to 150°C with a heating rate of 2°C/min. The test was conducted under nitrogen atmosphere with a flow of 50 mL/min. The results were reported in J/g °C.

2.4.1.3 THERMAL CONDUCTIVITY

Thermal diffusivity measurement was conducted according to flash method with Anter/TA Instruments DLF-2 flash system. The laser pulse was sent on the specimen and the temperature rise in the rear side of the sample was measured. From the obtained result, the baseline and the maximum rise to give the temperature difference ΔT_{max} . The time from initiation of pulse to reach $\Delta T_{1/2}$ was determined. The determined time is called the half time, $t_{1/2}$. Then with the help of Equation 31, the

diffusivity was calculated. Once the diffusivity calculated, the thermal conductivity is calculated by Equation 31.

$$\alpha = 0.13879 \frac{L^2}{t_{1/2}} \quad (30)$$

$$\lambda = \alpha \times Cp \times \rho \quad (31)$$

During diffusivity determination, the sample pieces were used from section 2.3. The slices were cut with a punch with a radius of 12.7 mm to the dimensions defined for the required geometry. The flash method requires a thickness of 1.5 – 2 mm, a radius of 12.7 mm.

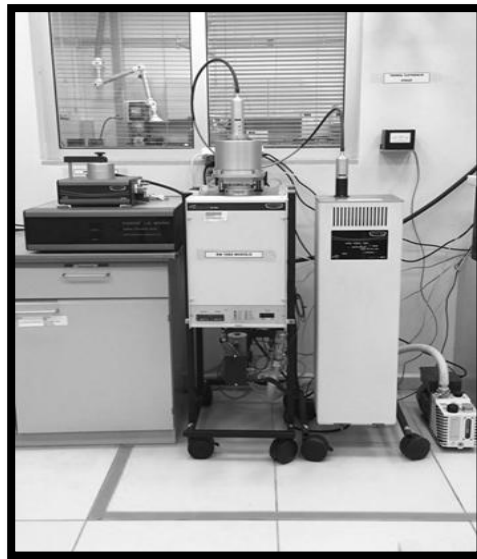


Figure 33 TA Instruments Thermal Conductivity

Sample's thickness was measured with a calibrated caliper. The both sides of the sample were coated with graphite spray to enable efficient absorption of laser beam. Samples were tested at 30°C with 3 laser shots under nitrogen. The test was conducted according to ASTM E1461 – 01. The average results were reported in W/mK.

2.4.1.4 COEFFICIENT OF LINEAR THERMAL EXPANSION, CTE

The coefficient of linear thermal expansion (CTE) was determined with Rheometric Scientific TMA 500. CTE is calculated from the dimensional change occurred in the sample upon heating with Equation 32.

$$\alpha_m = \frac{\Delta L_{sp} \times k}{L \times \Delta T} \quad (32)$$

$$k = \frac{\alpha_{ref} \times L_{ref} \times \Delta T_{ref}}{\Delta L_{ref}} \quad (33)$$

Where;

α_m : Mean coefficient of linear thermal expansion $\mu\text{m} / (\text{m}^\circ\text{C})$

α_{ref} : mean coefficient of linear thermal expansion, for reference, $\mu\text{m} / (\text{m}^\circ\text{C})$

k : Calibration coefficient

L : Specimen length at room temperature, m

ΔL_{ref} : Change of reference material length due to heating, μm

L_{ref} : Reference material length at room temperature, m

ΔL_{sp} : Change of specimen length, μm

During CTE determination, the sample pieces were used from section 2.3. The test was conducted according to ASTM Standard E 831 – 03. A cubic sample with the dimensions 10×10×5 mm was prepared and tested from -100°C to 200°C with a heating rate of 5°C/min. The test was conducted under nitrogen with 100 mL/min flow, by using flat expansion probe and 5 g of load. The results were reported in $\mu\text{m}/\text{m}^\circ\text{C}$.



Figure 34 Rheometric Scientific TMA 500

2.4.1.5 DECOMPOSITION TEMPERATURE

In the decomposition temperature determination TA Instruments Q500 TGA was used. The conversion percentage of the propellant was calculated according to Equation 34. The decomposition step was determined by the plotting the derivative of % weight change according to temperature.

$$W = \frac{\Delta m}{m_0} \times 100 \quad (34)$$

During decomposition temperature determination, the sample pieces were used from section 2.3. 1.39 mg of propellant was weighed into a previously tared platinum TGA pan. By using brass tweezers, sample pan was placed into the sample platform of the instrument.

The sample was tested from 25°C to 900°C with a heating rate of 20°C/min. The test was conducted according to STANAG 4515. The test was carried out under nitrogen atmosphere with a flow of 60 mL/min. The decomposition temperature was reported in °C and weight change was reported in %.



Figure 35 TA Instruments TGA Q 500

2.4.2 RHEOLOGICAL CHARACTERIZATION

2.4.2.1 GLASS TRANSITION TEMPERATURE, T_g

The glass transition temperature was determined with TA Instruments ARES G2 rheometer. The torsion rectangular geometry was used. The storage modulus versus temperature graph was plotted. The T_g is calculated according to the decrease in the storage modulus. Two tangent lines were drawn. First tangent was drawn before the transition and the second tangent was drawn after the transition, from the midpoint of the storage modulus decrease. The intersection of these plots was reported as T_g .

During glass transition temperature determination, the sample pieces were used from section 2.3. The propellant was cut into pieces with a razor blade into the defined geometry. The torsion rectangular geometry requires a length of 50 – 55 mm, width of 12.5 – 13 mm and thickness of 2 – 3 mm. The dimensions (length, thickness and width) were measured with a caliper and put into the software. The test was conducted according to ASTM D 7028 Glass Transition Temperature of Polymer Matrix Composites by Dynamic Mechanical Analysis. The conditions were given in Table 2.

Table 2 Test conditions for glass transition temperature (T_g)

TEST NAME	TEST CONDITIONS	
T_g	Temperature Range:	-130°C/-45°C
	Temperature Ramp Rate:	2 °C/min
	Frequency:	1 Hz
	Strain:	0.1 %

2.5 DETERMINATION OF MASTER CURVE BY RHEOMETER

The master curve was determined with TA Instruments ARES G2 rheometer. The torsion rectangular geometry was used. The time-temperature superposition principle was used to generate the master curve. The shift factors were calculated according to WLF equation given in section 1.4.8. The reference temperature was chosen as 20°C. In addition to this, the shift factors and the activation energy were also determined according to the Arrhenius principle given in 1.4.8.4.

The final sample dimensions were measured with a calibrated caliper. Each sample was mounted to torsion geometry and conditioned at -60°C for 10 minutes to enable homogeneous temperature distribution. After conditioning, the sample was fixed with the recommended torque value by the manufacturer TA Instruments (60 cNxm).

To be able to determine the strain value for testing, the propellant was subjected to frequency sweeps at 4 different strain values (0.2%, 0.5%, 1% and 2%).

The test conditions are given in Table 3 were applied during all tests and they were given in Table 3. Auto tension mode was activated and 1 N of axial force was applied on the sample to protect the sample from any shrinkage or expansion features may originate from temperature change. The strain was set to 2 %.

Table 3 Test conditions for rheometer

<u>TEST CONDITIONS</u>	
Temperature Range:	-60°C/60°C
Temperature Step:	20°C
Frequency Range:	100 – 0.01 Hz
Strain:	2%

Heating process was done with air circulation in the rheometer oven and cooling process was done with liquid nitrogen for each test. Obtained results were investigated with the help of ARES G2 Trios software. Shift factors, A, B constants and storage modulus versus reduced time plot and activation energy in kJ/mol were reported.

2.6 DETERMINATION OF MASTER CURVE BY UNIVERSAL MECHANICAL TEST SYSTEM

The stress relaxation tests were carried out with Instron 4481 mechanical testing instrument. A 1 kN capacity calibrated, certified load cell was used. Roller grips were used to attach the samples. Cooling process was carried out under liquid nitrogen in an environmental chamber which is capable of working in the temperature range of -150°C to 250°C.



Figure 36 Instron 4481 50kN Tensile Testing System

The stress relaxation curves were obtained by applying 2% strain on the specimen and monitoring the stress over time. Resultant curves were shifted according to time temperature superposition principle. Shift factors were calculated with WLF equation given in 1.1.7. The reference temperature was chosen as 20°C. Untabbed samples were used. The 1 cm thick slices obtained in section 2.3 were further cut with a punch in the shape of a dog bone (Figure 37).

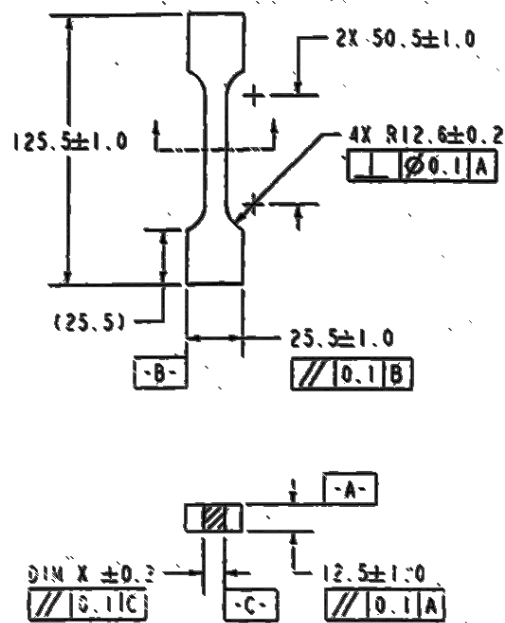


Figure 37 Specimen Configuration

The sample punch was used has JANNAF type dimensions. The prepared test sample was wrapped into aluminum foil and stored in the desiccator until testing. Before the test, each sample was measured with a micrometer for thickness, width and length.

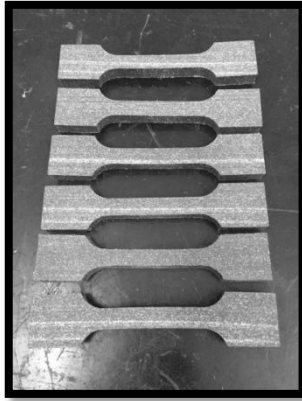


Figure 38 Dog bone samples for stress relaxation tests

The sample sizes were approximately 10 mm in thickness and in width. Gauge length used was around 69 mm.

The stress relaxation tests given in the Table 4 at 7 different temperatures (-60 °C / -40 °C / -20 °C / 0 °C / 20 °C / 40 °C / 60 °C) were carried out to obtain the master curve. For each test condition (temperature) 3 specimens were used.

Table 4 Stress Relaxation Test Conditions

<u>TEST NAME</u>	<u>TEST CONDITION</u>	
Stress Relaxation	Test Temperature	: -60 °C / -40 °C / -20 °C / 0 °C / 20 °C / 40 °C / 60 °C
	Cross Head Speed	: 50 mm/min
	Relaxation Time	: 2 Hours
	Strain	: 2 %

Test was carried out according to a military NATO standard STANAG 4507. Calculation of shift factors and A & B constants were done manually. Shifting of relaxation curves were done with the help of Microsoft Excel software. The stress versus time plots at different temperatures, relaxation modulus versus reduced time plot, shift factors and A & B constants were reported.

CHAPTER 3

RESULTS AND DISCUSSION

In this study, the propellant was characterized thermally, rheologically and mechanically. The thermal characterization parameters like autoignition temperature, specific heat, thermal conductivity, coefficient of linear thermal expansion and decomposition temperature, were important to understand thermal behavior of the propellant, to provide information about limits of working range for mechanical tests and provide information for the *structural analysis and test department* in ROKETSAN. This department uses the data in further modeling studies for propellant behavior. Moreover, thermal analysis data provided information about the conditions for rheological and mechanical characterization.

The obtained results were evaluated according to demands of the customer. The customer defines the operating purpose, range and conditions. In the limits of customer demands, *the structural analysis and test department* in ROKETSAN determines acceptance criteria for the tests. The following test results were compared according to these critical values.

Besides thermal characterization, rheological tests were conducted. The glass transition temperature and master curve of the propellant were determined by the rheometer.

Finally, the propellant was subjected to mechanical tests. Mechanical properties were used to generate the master curve and shift factors. These data obtained were compared to master curve constructed by rheometer.

3.1 DETERMINATION OF AUTOIGNITION TEMPERATURE

The autoignition temperature of the propellant was determined according to section 2.4.1.1 (See section 2.4.1.1). As a result of this test, the autoignition was detected as 350°C and given in Figure 39. The propellant releases 1185 J/g energy upon ignition. The sample amount used in the test was very low (< 5mg) because high amount of energy is released in short time and it can destroy the test system used. The onset of autoignition temperature was consistent with decomposition temperature.

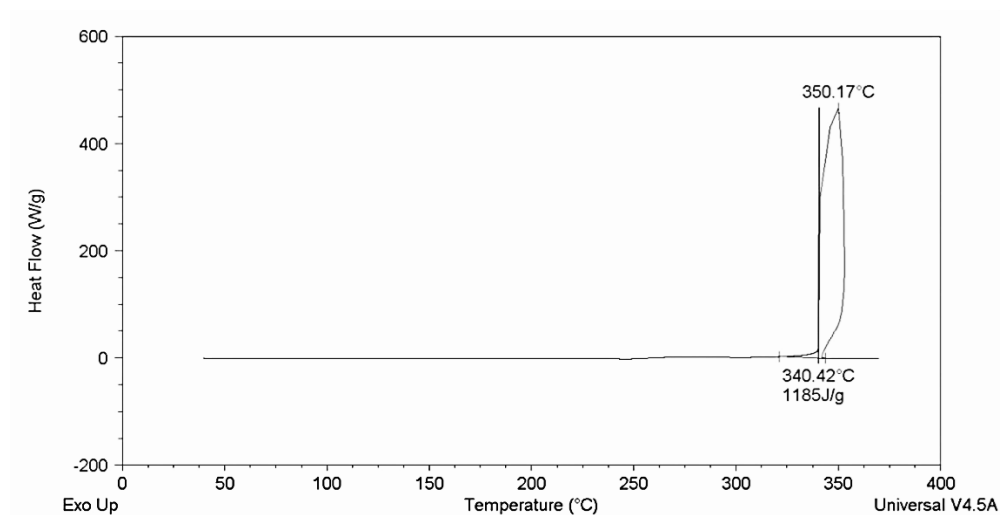


Figure 39 Autoignition thermogram for the given propellant

3.2 DETERMINATION OF SPECIFIC HEAT, C_p

The specific heat determination was carried out according to section 2.4.1.2 (See section 2.4.1.2). The results were calculated between -40°C to 60°C and given in Figure 41. This temperature interval was chosen because the rocket motor will operate under similar environmental conditions. It can be observed that, as temperature increases, specific heat increases. At 20°C , 1.05 J energy is required to increase the 1 g of sample by 1°C . As temperature increases from -60°C to 80°C , the specific heat increases from $0.91 \text{ J/g}^{\circ}\text{C}$ to $1.14 \text{ J/g}^{\circ}\text{C}$. The increase in specific heat as temperature increases was expected and the determined C_p values were acceptable.

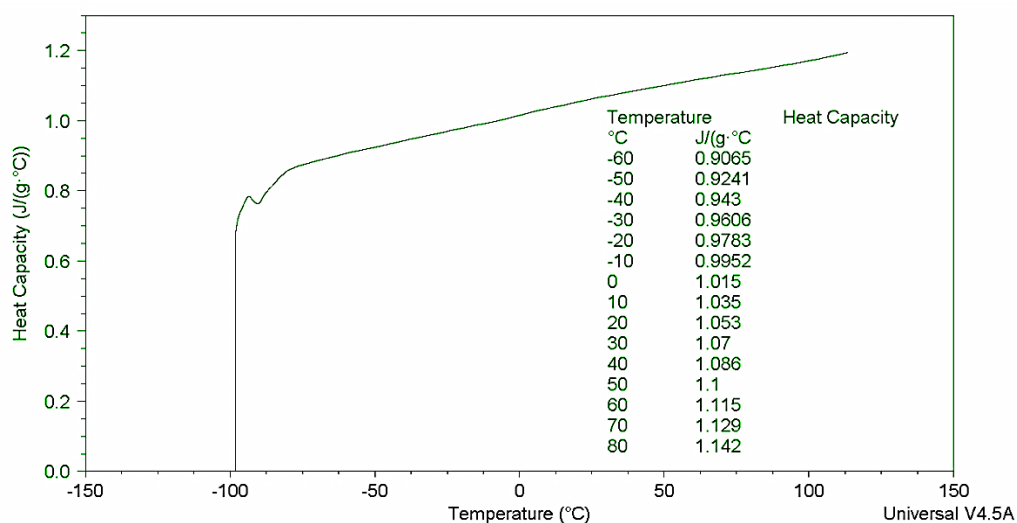


Figure 40 Heat capacity of the given propellant within the temperature range of -60°C to 80°C

3.3 DETERMINATION OF THERMAL CONDUCTIVITY

The thermal diffusivity was calculated according to the procedure given in 2.4.1.3 (See section 2.4.1.3). The diffusivity result was $0.019 \text{ cm}^2/\text{s}$ at 30°C and given in Figure 42. The thermal conductivity was then calculated using Equation 31. The density of the propellant is 1.7 g/cm^3 at 30°C . The specific heat data was obtained from section 3.2. It was 1.07 J/g at 30°C .

Then by Equation 31, the thermal conductivity was calculated as 0.346 W/mK . The calculated result was acceptable and consistent with other composite propellants manufactured in ROKETSAN.

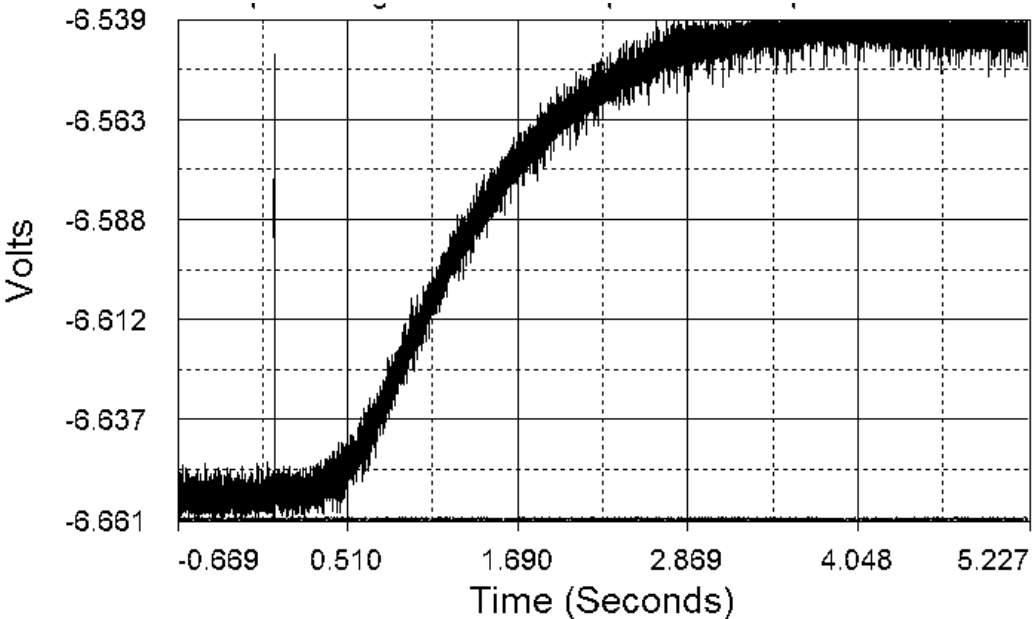


Figure 41 The voltage versus time graph for calculation of thermal conductivity

3.4 DETERMINATION OF COEFFICIENT OF LINEAR THERMAL EXPANSION, CTE

The coefficient of linear thermal expansion was determined according to the procedure given in 2.4.1.4 (See section 2.4.1.4). The CTE was calculated in between the temperature range of -40°C to 100°C . The temperature range was selected according to working conditions of rocket motor. The propellant did not show any transition in this range. It means that, the selected temperature range was appropriate to calculate CTE. The average CTE was calculated as $109.22 \mu\text{m}/\text{m}^{\circ}\text{C}$. The obtained result was used in the calculation of the thermal stress on the propellant and expansion was reasonable.

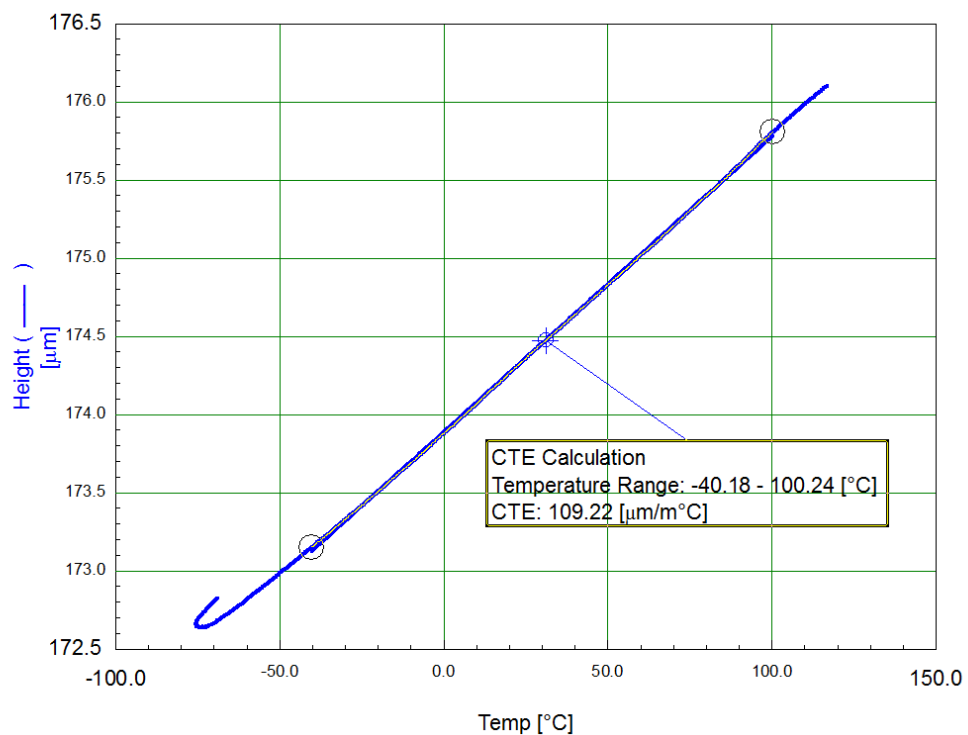


Figure 42 CTE of the given propellant between -40°C to 100°C .

3.5 DECOMPOSITION TEMPERATURE

The decomposition temperature was determined according to 2.4.1.5 (See section 2.4.1.5). The result is given in Figure 43. The maximum peak derivative was calculated as 345°C. The decomposition temperature calculated was consistent with the autoignition temperature. Upon ignition the propellant loses weight and release volatile gases. These volatile gases were not analyzed since it exceeds the capabilities of *material characterization laboratory* in ROKETSAN.

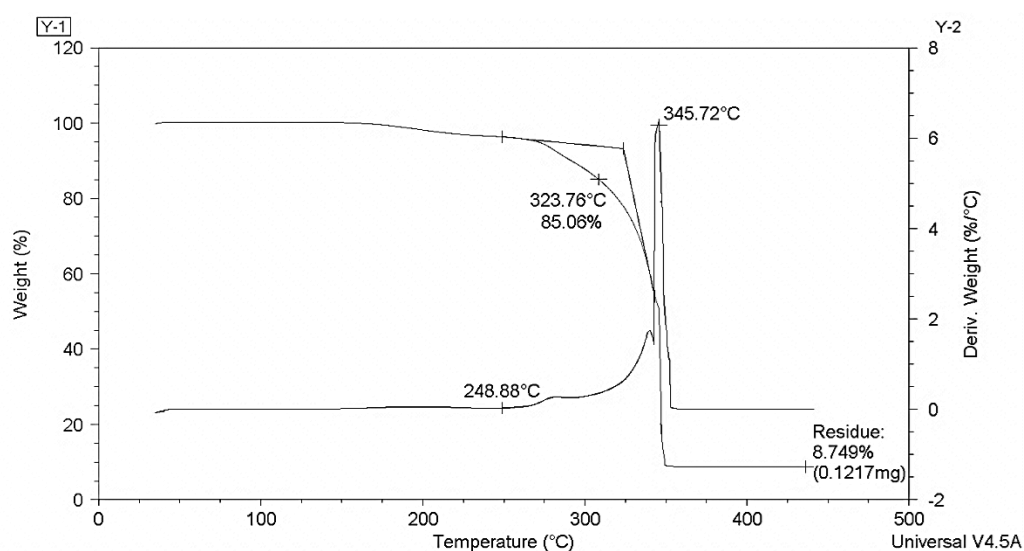


Figure 43 Decomposition temperature of the given propellant

3.6 DETERMINATION OF GLASS TRANSITION TEMPERATURE

The glass transition temperature of the propellant was determined using dynamic measurement as given in section 2.4.2.1 (See section 2.4.2.1). The test was carried out in the temperature range of -130°C to -45°C with 1 Hz frequency and 0.1 % strain. The glass transition temperature was calculated by the drop in the storage modulus. It was calculated as -87.3°C .

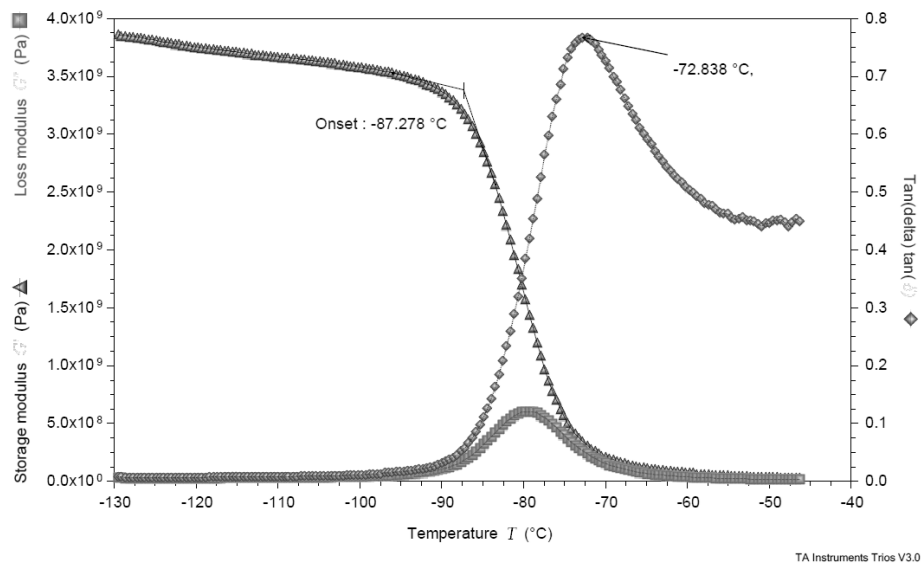


Figure 44 A typical dynamic mechanical test result for the propellant

Since for the given propellant the glass transition temperature was -87.3°C , the minimum test temperature for other characterization techniques was selected as -60°C .

3.7 DETERMINATION OF MASTER CURVE BY RHEOMETER

3.7.1 DETERMINATION OF EXPERIMENTAL CONDITIONS FOR RHEOMETER TESTS

The generation of master curve by rheometer was conducted according to the procedure given in 2.5 (See section 2.5).

Before generation of the master curve, the linear viscoelastic region for the propellant was determined. The linearity of the working range was proved by the frequency sweeps conducted at 0.2%, 0.5%, 1% and 2% strain, in the range of 100 – 0.01 Hz.

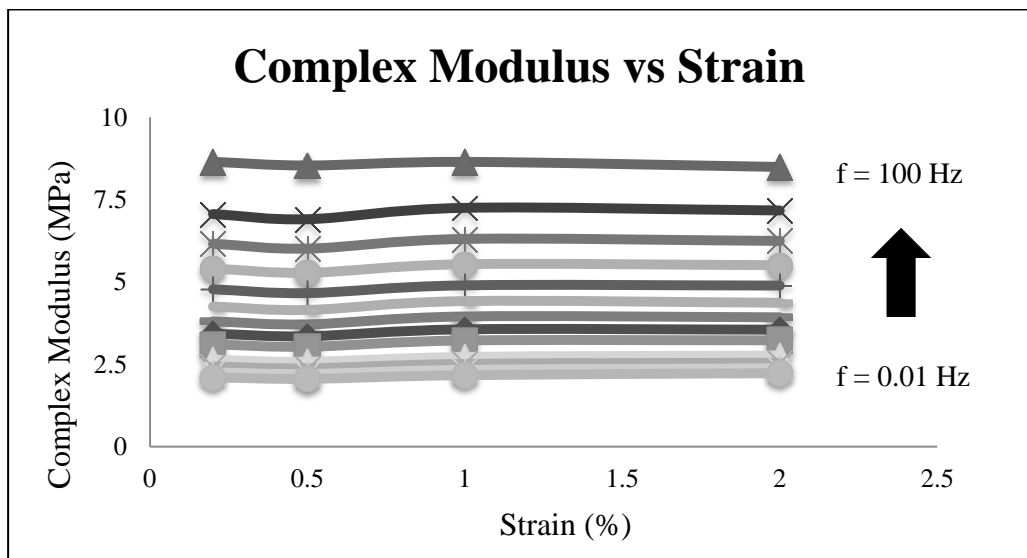


Figure 45 Amplitude comparison at 0.2%, 0.5%, 1% and 2% strain at 20° at different frequencies.

It was observed that, the complex modulus was not affected by the applied strain range (0.2% to 2%, Figure 45). According to this data, the strain was kept same with mechanical test conditions and it was chosen as 2%.

To be able to compare two methods, rheometer and mechanical tests, rheometer parameters were set similar to mechanical tests.

The temperature range was selected in between -60°C to 60°C . It was set according to the operating conditions for the propellant in a motor case and adjusted to simulate same temperature transitions in stress relaxation tests. In this temperature range, it was proved by thermal tests previously conducted, the propellant exhibits no decomposition or phase change.

The rheometer was set to temperature sweep mode. At this mode, the temperature ramp rate has no effect on the measurement. The instrument heats to the temperature of interest, and then it starts to take data after temperature equilibration for 5 min. Therefore, temperature steps were chosen as $20^{\circ}\text{C}/\text{min}$ to optimize the test duration and to simulate the same increments with mechanical tests. The frequency range was selected as 0.01 – 100 Hz.

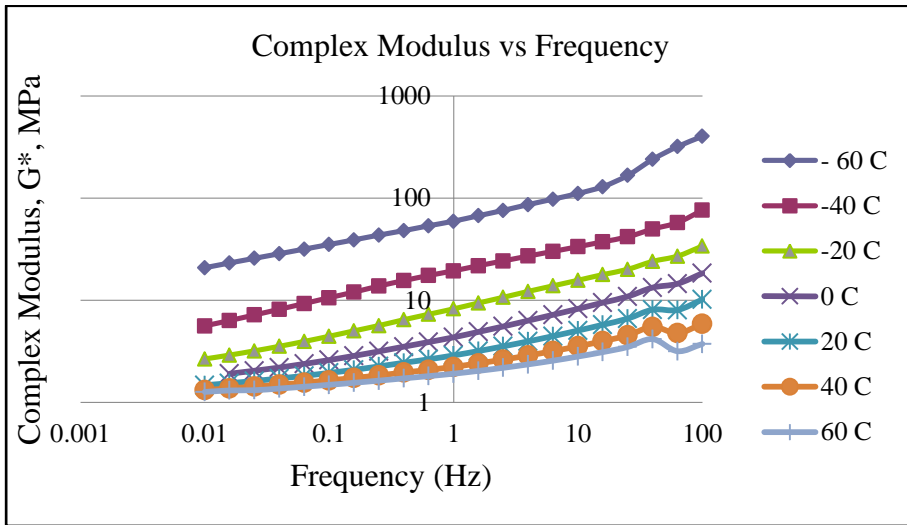


Figure 46 Complex modulus versus frequency data for rheometer results

The obtained frequency sweep test results were shifted experimentally by ARES G2 rheometer Trios software.

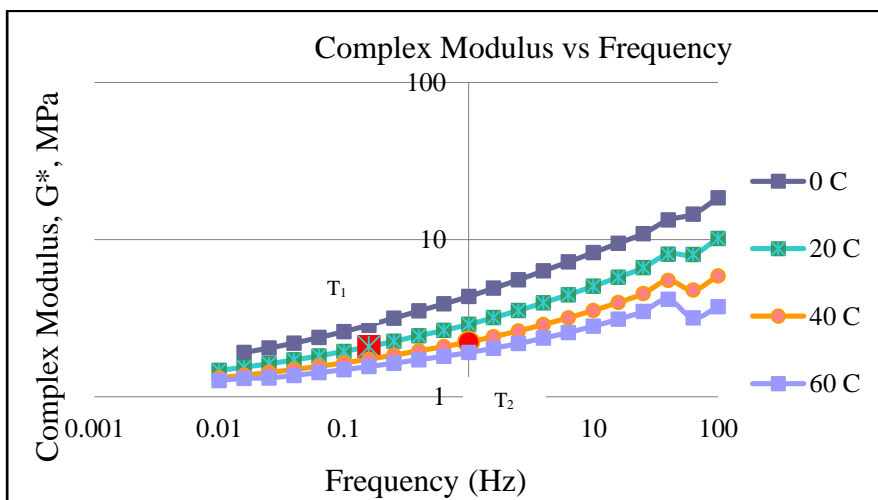


Figure 47 Experimental shift factor calculation

As given in Figure 47, the same modulus value on different temperature curves (marked with red color on Figure 47) was chosen. The time values at different temperature curves were noted for the selected modulus value. Then the shift factor was calculated as the ratio of the two time values $\frac{T_2}{T_1}$.

Table 5 Experimental shift Factors by rheometer

TEMPERATURE (°C)	log a_T
-60 °C	5.10
-40 °C	3.15
-20 °C	1.85
0 °C	0.80
20 °C	0.00
40 °C	-0.70
60 °C	-1.27

After calculation of experimental shift factors, the WLF equation (Equation 35) was used to calculate the constants A and B.

The constants A and B were calculated with the linearized and generalized WLF equation (Equation 35) since the reference temperature was not selected as T_g .

$$-\frac{T-T_{Ref}}{\log a_T} = \frac{B}{A} + \frac{1}{A}(T - T_{Ref}) \quad (35)$$

The $-\frac{T-T_{Ref}}{\log a_T}$ vs $(T - T_{Ref})$ graph was plotted and given in Figure 48. From the slope the constant A and then from the intercept the constant B was calculated.

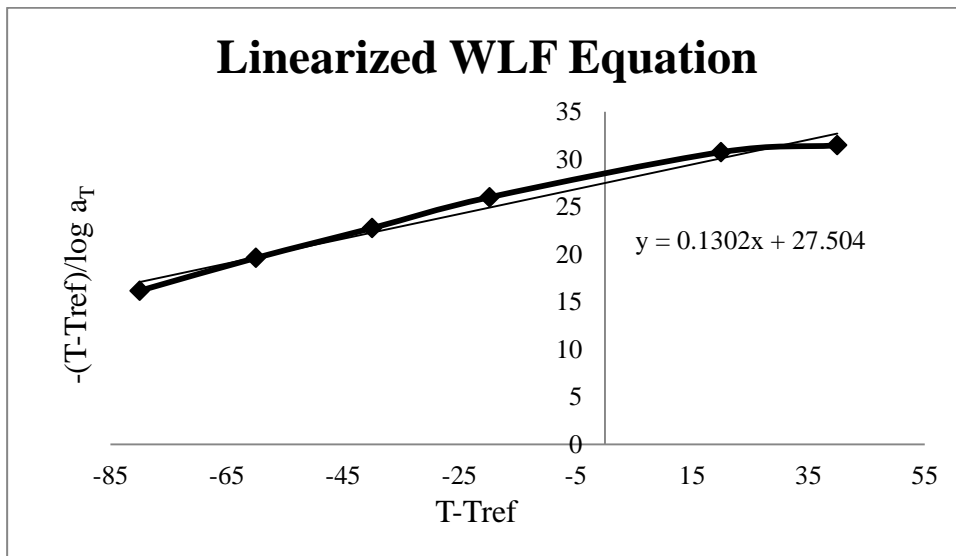


Figure 48 Linearized WLF equation for rheometer shift factors

$$\text{Slope} = \frac{1}{A} = 0.1302, A = 7.68$$

$$\text{Intercept} = \frac{B}{A} = 27.504, B = 211.24$$

After calculation of WLF equation constants with experimental data, the shift factors were calculated with Equation 35 by substituting the A, B constants and the temperature values.

Table 6 Shift Factors calculated by WLF equation for rheometer

<u>TEMPERATURE (°C)</u>	<u>log a_T</u>
-60 °C	4.68
-40 °C	3.04
-20 °C	1.79
0 °C	0.79
20 °C	0.00
40 °C	-0.66
60 °C	-1.22

Finally, the master curves were generated with the conditions given in Table 7 and with both experimental and WLF shift factors (Table 5 and 6).

Table 7 WLF constants according to performed test conditions

	<u>TEST CONDITIONS</u>
Temperature	-60°C/60°C
Temperature Step	20 °C/min
Frequency Range	100-0.01 Hz
A	7.68
B	211.2

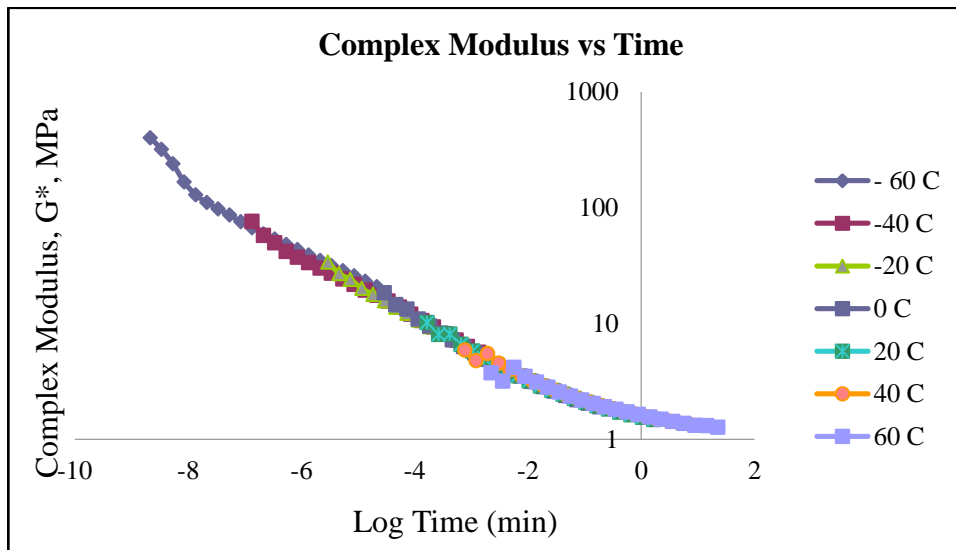


Figure 49 Master curve obtained with experimental shift factors (Table 5)

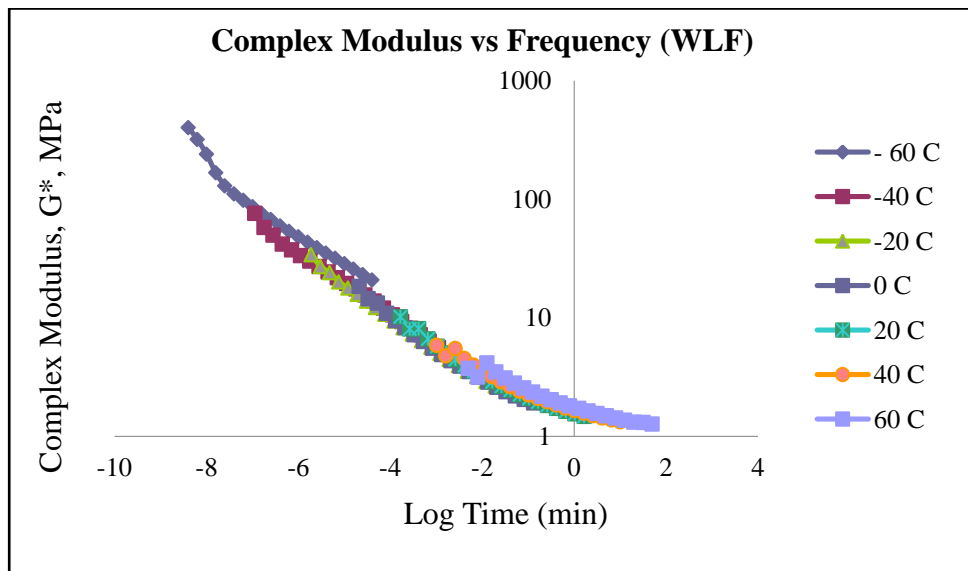


Figure 50 Master curve obtained with WLF shift factors (Table 6)

In Figure 49, the master curve obtained with experimental shift factors was given and in Figure 50, the master curve with WLF shift factors was given. By looking at two plots, one can visually predict that the experimental shift factors had better fitting according to WLF shift factors. The comparison of the shift factors were given in Table 8. Since the experimental shift factors results in a better master curve, these factors were used in mechanical testing comparison.

Table 8 Representation of shift factors by WLF equation

<u>TEMPERATURE</u> °C	<u>log a_T</u> <u>(EXP.)</u>	<u>log a_T</u> <u>(WLF)</u>	<u>% ERROR</u>	<u>RSS</u>
-60°C	5.10	4.68	8.24	0.176
-40°C	3.15	3.04	3.49	0.012
-20°C	1.85	1.79	3.24	0.004
0°C	0.80	0.79	1.25	0.000
20°C	0.00	0.00	0.00	0.000
40°C	-0.70	-0.66	5.71	0.002
60°C	-1.27	-1.22	3.94	0.003

3.7.2 ARRHENIUS RELATION FOR RHEOMETER DATA

Besides Williams – Landel – Ferry equation, it is possible to use Arrhenius equation for calculation of the shift factors and activation energy. Firstly, the activation energy given in Equation 36 was calculated by substituting experimental shift factors (Table 5).

The activation energy of the propellant was calculated as the slope of the $\ln a_T$ versus $\left(\frac{1}{T} - \frac{1}{T_0}\right)$ graph. The result was 68.95 kJ/mol with R^2 0.99, $T_{\text{reference}} = 20^\circ\text{C}$.

$$\ln a_T = \left(\frac{E_a}{R}\right) \times \left(\frac{1}{T} - \frac{1}{T_0}\right) \quad (36)$$

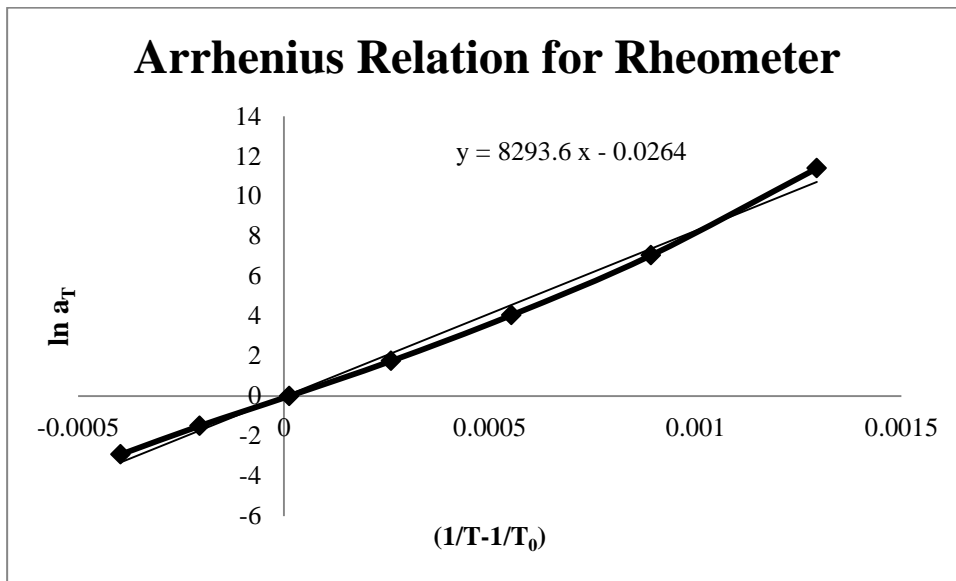


Figure 51 $\ln a_T$ versus $\left(\frac{1}{T} - \frac{1}{T_0}\right)$ plot for calculation of the activation energy

As it is given in Figure 51, slope of the $\ln a_T$ versus $\left(\frac{1}{T} - \frac{1}{T_0}\right)$ graph is 8293.6 which is equal to $\frac{E_a}{R}$. From this relation the activation energy is equal to slope times the gas constant ($m = \frac{E_a}{R}$). The universal gas constant was 8.314 J/K.mol. Therefore, the activation energy becomes $8293.6 \times 8.314 = 68952.9$ J/mol = 68.95 kJ/mol. After calculation activation energy, the shift factors by were calculated once again using Equation 36 and given in Table 9.

Table 9 Representation of shift factors by Arrhenius equation

<u>TEMPERATURE</u> °C	<u>log a_T</u> (Exp.)	<u>log a_T</u> (Arrh.)	<u>% ERROR</u>	<u>RSS</u>
-60°C	5.10	4.62	9.41	0.23
-40°C	3.15	3.17	0.63	0.00
-20°C	1.85	1.94	4.86	0.01
0°C	0.80	0.90	12.5	0.01
20°C	0.00	0.00	0.00	0.00
40°C	0.70	-0.79	12.9	0.01
60°C	-1.27	-1.48	16.5	0.04

The master curve was obtained by using the shift factors given in Table 9 and given in Figure 52. It was compared to the master curve obtained with experimental shift factors.

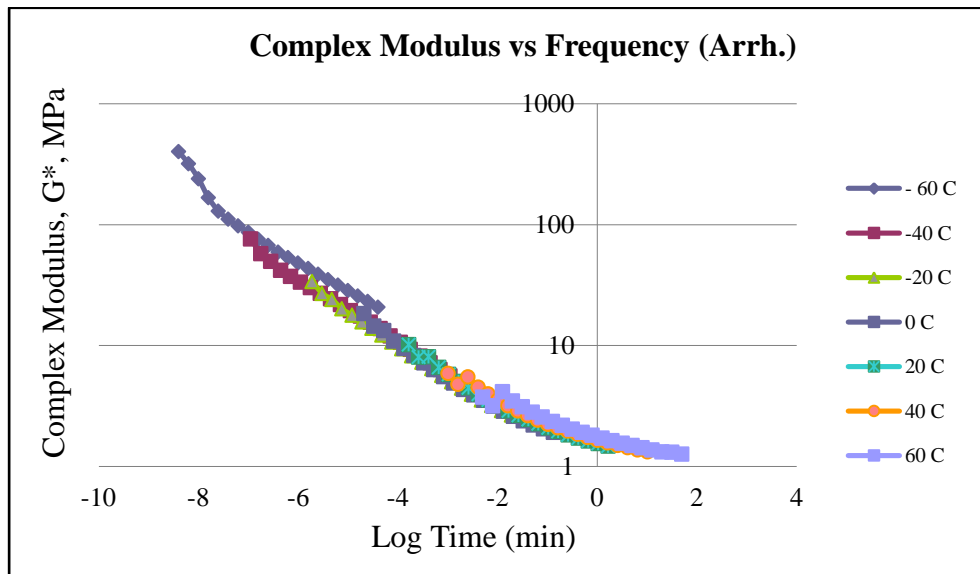


Figure 52 Master curve obtained with shift factors calculated by Arrhenius relation

From Figure 52, it can be concluded that the Arrhenius shift factors had similar effects as WLF shift factors on shifting (Table 10). As a result, the experimental shift factors were used in comparison with mechanical testing.

By using shift factors calculated from both WLF and Arrhenius equations, the residual sum of squares (RSS) was estimated (Table 10). Since WLF equation had lower RSS, it was concluded that, WLF approach was appropriate for data analysis.

Table 10 Comparison of experimental, WLF and Arrhenius shift factors

<u>Temperature</u> °C	<u>log a_T</u> <u>(Exp.)</u>	<u>log a_T</u> <u>(WLF)</u>	<u>log a_T</u> <u>(Arrh.)</u>	<u>RSS</u> <u>(WLF)</u>	<u>RSS</u> <u>(Arrh.)</u>
-60°C	5.10	4.68	4.62	0.176	0.230
-40°C	3.15	3.04	3.17	0.012	0.000
-20°C	1.85	1.79	1.94	0.004	0.008
0°C	0.80	0.79	0.90	0.000	0.010
20°C	0.00	0.00	0.00	0.000	0.000
40°C	-0.70	-0.66	-0.79	0.002	0.008
60°C	-1.27	-1.22	-1.48	0.003	0.044
				Sum of Squares	
				0.1963	0.3011

3.7.3 TIME – TEMPERATURE SUPERPOSITION (TTS) VALIDITY

The validity of the master curve can be checked by plotting phase angle versus complex modulus as described in 1.4.8.3 (Van Gulp Palmen plot). If the master curve is valid and conditions are accurate the Van Gulp Palmen plot should fall into a single curve as given in Figure 53.

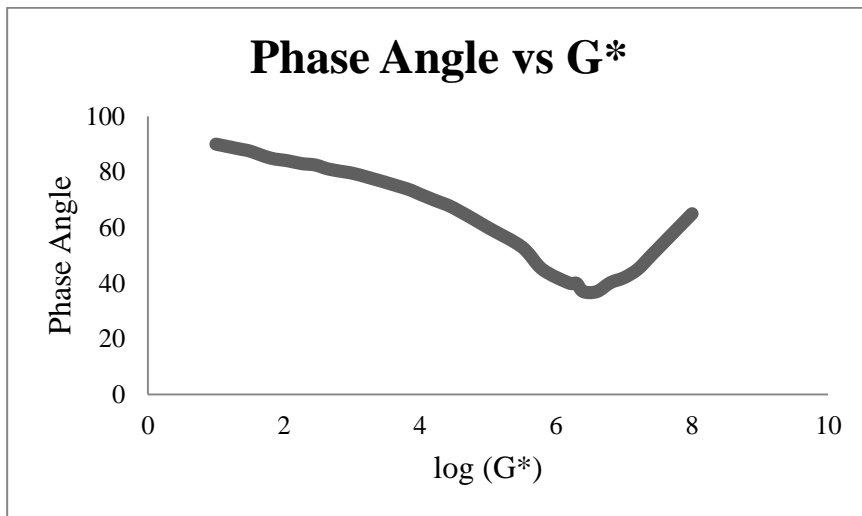


Figure 53 Illustration of Van Gurr Palmen plot (Gurr M., and Palmen J., 1998)

For the results obtained from the rheometer, the Van Gurr Palmen plot was established. From Figure 54, it can be observed that, the rheometer analysis holds and the Van Gurr Palmen plot falls into a single, non – deviated curve.

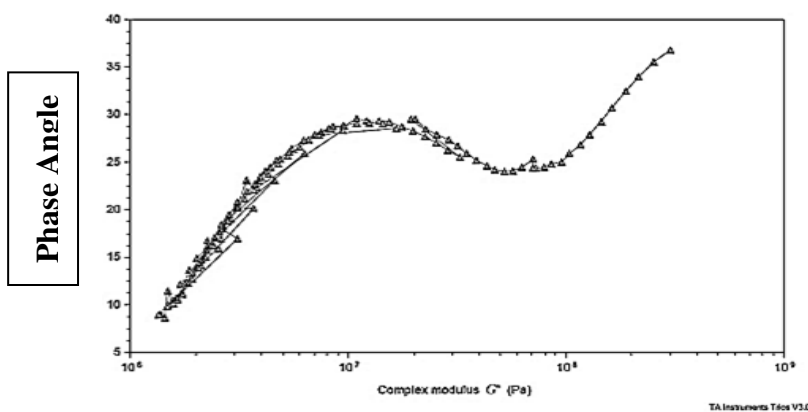


Figure 54 Van Gurr Palmen plot for rheometer data (Phase angle versus complex modulus)

3.7.4 REFERENCE TEMPERATURE SELECTION

In generation of master curve, since the WLF and Arrhenius equations were used to calculate the shift factors, the selection of reference temperature gains importance. The curves obtained are shifted according to a selected temperature.

In this study, the reference temperature was used as the room temperature which was simulating the mechanical tests.

3.8 DETERMINATION OF MASTER CURVE BY MECHANICAL TESTS

3.8.1 DETERMINATION OF EXPERIMENTAL CONDITIONS FOR MECHANICAL TESTS

At the beginning, the test conditions for mechanical testing were determined. These conditions were selected according to T_g and working conditions of the propellant. The strain value was set to 2% to represent the required deformation but at the same time to prevent application of over strain which may cause debonding and dewetting in the motor case (Table 11).

Table 11 Test Conditions for Mechanical Tests

<u>TEST NAME</u>	<u>TEST CONDITION</u>	
Stress Relaxation	Test Temperature:	-60°C/-40°C/-20°C/0°C/20°C/40°C/60°C
	Cross Head Speed:	50 mm/min
	Relaxation Time:	2 Hours
	Strain:	2 %

Stress relaxation tests were performed to calculate equilibrium modulus and shift factor. The test duration was 2 hours to see the total relaxation. At each test condition (temperature) 3 specimens were used. The results are given in section 3.9.

3.9 MECHANICAL TEST RESULTS

Acquired data from mechanical tests were treated according to the military standard STANAG 4507. The time when the specimen reached to maximum load was determined. This time value was multiplied by 10. Stress relaxation curves were used further from this time value to the final time value (Figure 55).

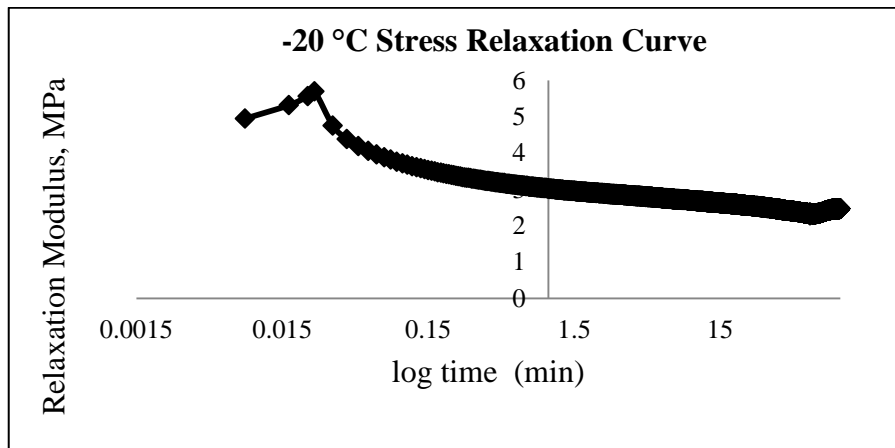


Figure 55 A typical stress relaxation curve obtained at -20°C.

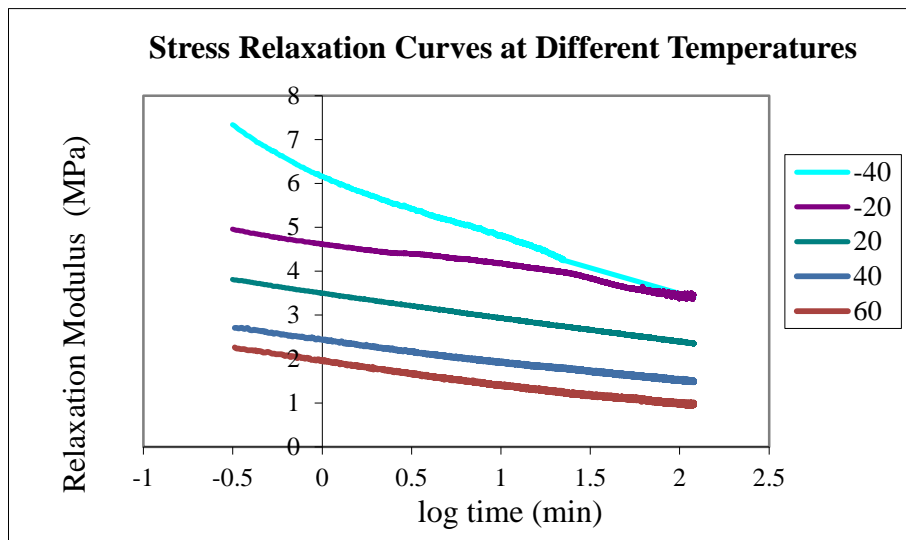


Figure 56 Stress relaxation curves at different temperatures

For the propellant used, there were certain quality criteria determined set by *explosives and propellant technologies department*. These values were determined according to the customer demand and operation principle of the rocket. In the analysis carried out by *the structural test analysis department*, the -60°C and 0°C results were deviated from the remaining data and they were not included in the master curve generation.

All curves obtained at different temperatures were treated in the same way. These curves were plotted in the same modulus vs time graph as illustrated in Figure 56. After that, the curve for room temperature ($T_{\text{reference}}$) was kept constant and other curves were shifted according to the shift factors calculated both by experimentally and by WLF equation.

The experimental shift factors were calculated in the same way as rheometer data and the results are given in Table 12. Since the data for -60°C and 0°C were excluded, the shift factors were not calculated.

Table 12 Experimental shift factors calculated from mechanical tests

<u>TEMPERATURE</u> °C	<u>log a_T (EXP.)</u>
-60 °C	-
-40°C	3.00
-20°C	1.70
0°C	-
20°C	0.00
40°C	-1.80
60°C	-2.70

As in section 3.7.1, the $-\frac{T-T_{Ref}}{\log a_T}$ vs $(T - T_{Ref})$ graph was plotted and given in Figure 57. From the slope the constant A and then from the intercept the constant B was calculated.

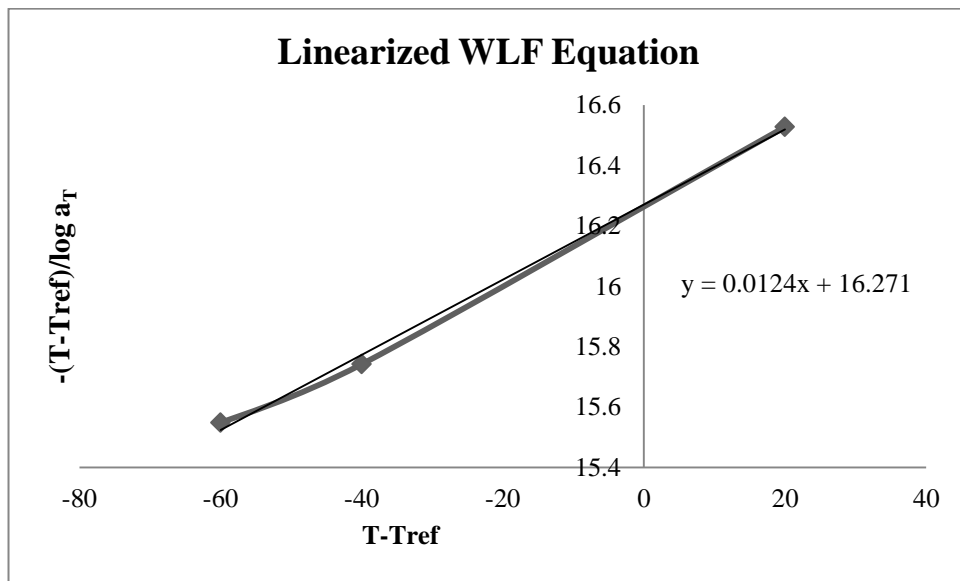


Figure 57 Linearized WLF equation for mechanical shift factors

$$\text{Slope} = \frac{1}{A} = 0.0124, A = 80.64$$

$$\text{Intercept} = \frac{B}{A} = 16.271, B = 1312$$

After calculation of WLF equation constants with experimental data, the shift factors were calculated with Equation 35 by substituting the A, B constants and the temperature values. The calculated WLF shift factors for mechanical testing were given in Table 13.

Table 13 Shift factors calculated by WLF equation for mechanical test results

<u>TEMPERATURE (°C)</u>	<u>log a_T</u>
-60 °C	-
-40 °C	3.86
-20 °C	2.53
0 °C	-
20 °C	0.00
40 °C	-1.21
60 °C	-2.39

Finally, the master curves were both generated using experimental shift factors and WLF shift factors.

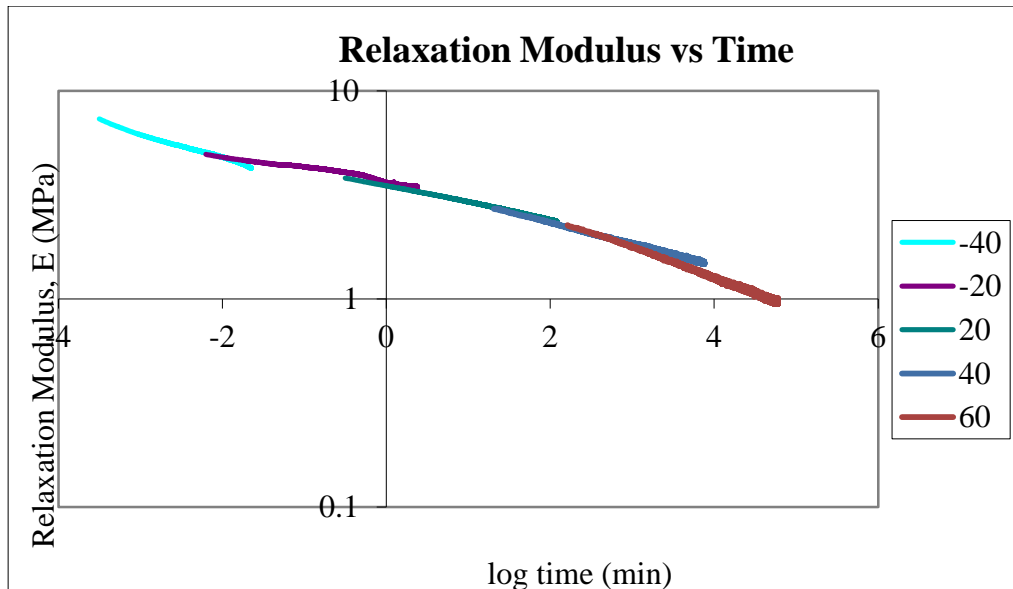


Figure 58 Master curve generated by using experimental shift factors

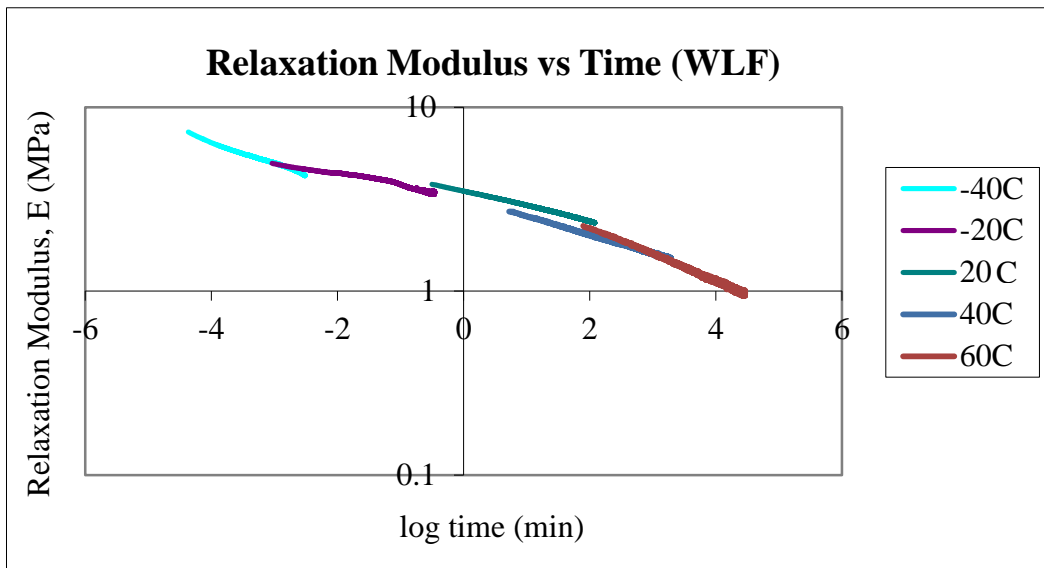


Figure 59 Master curve generated by using WLF shift factors

In Figure 58, the master curve obtained with experimental shift factors was given and in Figure 59, the master curve with WLF shift factors was given. By looking at two plots, one can visually predict that the experimental shift factors had better fitting according to WLF shift factors. The comparison of the shift factors were given in Table 14. Since the experimental shift factors results in a better master curve, these factors were used in mechanical testing comparison.

Table 14 Representation of shift factors by WLF equation

<u>TEMPERATURE</u> °C	<u>log a_T</u> <u>(EXP.)</u>	<u>log a_T</u> <u>(WLF)</u>	<u>% ERROR</u>	<u>RSS</u>
-60°C	-	-	-	-
-40°C	3.00	3.86	28.7	0.74
-20°C	1.70	2.53	48.8	0.69
0°C	-	-	-	-
20°C	0.00	0.00	0.00	0.00
40°C	-1.80	-1.21	32.8	0.35
60°C	-2.70	-2.39	11.5	0.10

3.9.1 ARRHENIUS RELATION FOR MECHANICAL TEST DATA

As in rheometer section, besides Williams – Landel – Ferry equation, it is possible to use Arrhenius equation for calculation of the shift factors and activation energy. Firstly, the activation energy given in Equation 36 was calculated by substituting experimental shift factors (Table 12).

As it is given in Figure 60, slope of the $\ln a_T$ versus $\left(\frac{1}{T} - \frac{1}{T_0}\right)$ graph is 11078 which is equal to $\frac{E_a}{R}$. From this relation the activation energy is equal to slope times the gas constant ($m = \frac{E_a}{R}$). The universal gas constant was 8.314 J/Kmol. Therefore, the activation energy becomes $11078 \times 8.314 = 92102 \text{ J/mol} = 92.10 \text{ kJ/mol}$ with $R^2 = 0.99$.

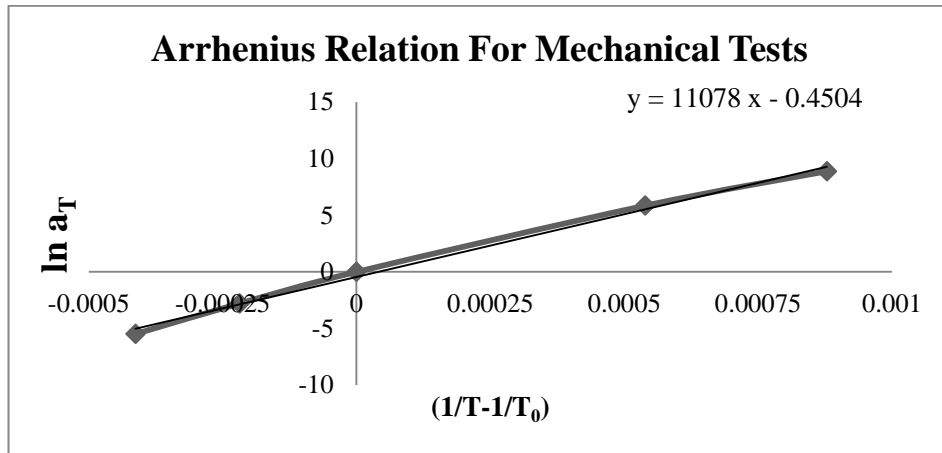


Figure 60 $\ln a_T$ versus $\left(\frac{1}{T} - \frac{1}{T_0}\right)$ plot for calculation of the activation energy

After calculation activation energy, the shift factors by were calculated once again using Equation 36 and given in Table 15.

Table 15 Representation of shift factors by Arrhenius equation

<u>TEMPERATURE</u> °C	<u>log a_T</u> <u>(EXP.)</u>	<u>log a_T</u> <u>(Arrh.)</u>	<u>% ERROR</u>	<u>RSS</u>
-60°C	-	-	-	-
-40°C	3.00	4.21	40.3	0.79
-20°C	1.70	2.59	52.3	-
0°C	-	-	-	0.00
20°C	0.00	0.00	0.00	0.56
40°C	-1.80	-1.05	41.7	0.53
60°C	-2.70	-1.97	27.0	1.46

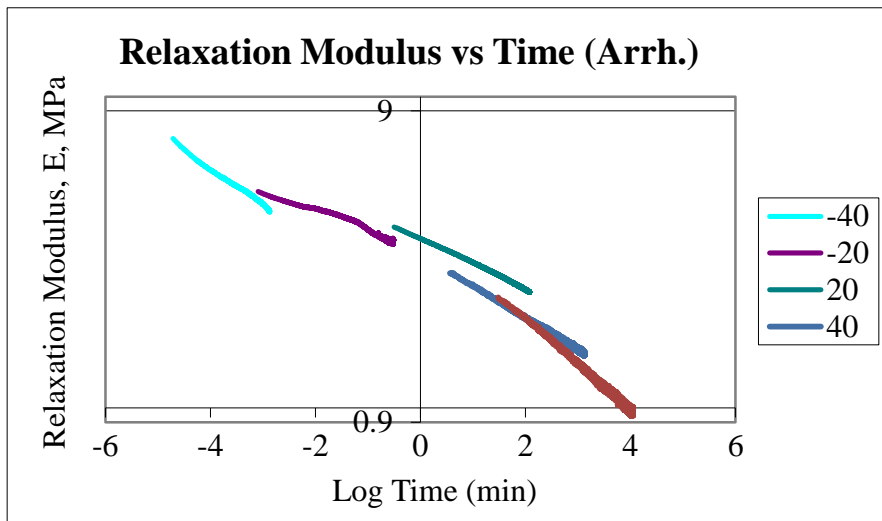


Figure 61 Master curve generated with Arrhenius Shift Factors for mechanical test results

From Figure 61, it can be concluded that the Arrhenius shift factors had worse effects as WLF shift factors on shifting (Table 16). As a result, the experimental shift factors were used in comparison with mechanical testing.

By using shift factors calculated from both WLF and Arrhenius equations, the residual sum of squares (RSS) was estimated (Table 16). Since WLF equation had lower RSS, it was concluded that, WLF approach was appropriate for data analysis.

Table 16 Comparison shift factors for mechanical testing

<u>TEMPERATURE</u> °C	<u>log a_T</u> <u>(EXP.)</u>	<u>log a_T</u> <u>(WLF)</u>	<u>log a_T</u> <u>(ARRH.)</u>	<u>RSS</u> <u>(WLF)</u>	<u>RSS</u> <u>(Arrh.)</u>
-60°C	-	-	-	-	-
-40°C	3.00	3.86	4.21	0.74	0.79
-20°C	1.70	2.53	2.59	0.69	-
0°C	-	-	-	-	0.00
20°C	0.00	0.00	0.00	0.00	0.56
40°C	-1.80	-1.21	-1.05	0.35	0.53
60°C	-2.70	-2.39	-1.97	0.10	1.46
				Sum of squares	
				1.87	3.35

3.10 COMPARISON OF MASTER CURVES AND SHIFT FACTORS

From the rheometer data, complex modulus was measured and in mechanical tests relaxation modulus was obtained. As a result, since the deformation modes are different, the obtained data cannot directly be compared. To be able to compare two moduli, Poisson's ratio was used. The propellant was assumed as an incompressible material. Therefore, the Poisson's ratio can be used as 0.5. Considering this assumption, Equation 38 can be derived from Equation 37:

$$G = \frac{E}{2(1+\nu)} \quad (37)$$

$$G = \frac{E}{3} \quad (38)$$

According to Equation 38, the shear modulus values E was calculated and these modulus values were used to compare two master curves. Every G value was multiplied by 3. In the rheometer data, the frequency (in Hertz) values were inversed to calculate time and reduced time was calculated ($\log(t) - \log(a_T)$). In Figure 62, the master curve obtained for rheometer was given.

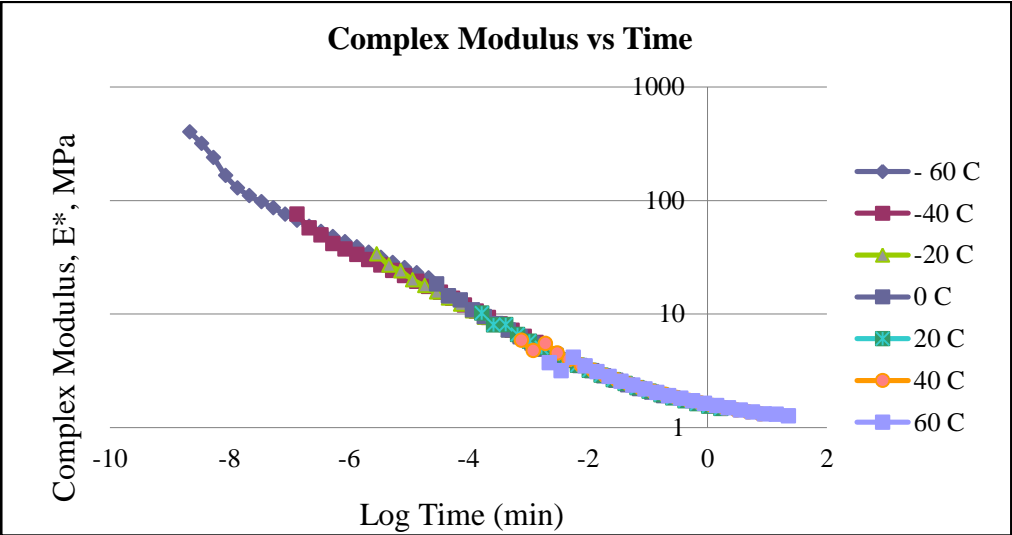


Figure 62 Master Curve obtained with rheometer (Complex shear modulus E^* vs reduced time)

The mechanical test results were plotted against reduced time. The experimental shift factors were used for shifting and the curve was given in Figure 63. The coincident curves were given in Figure 64.

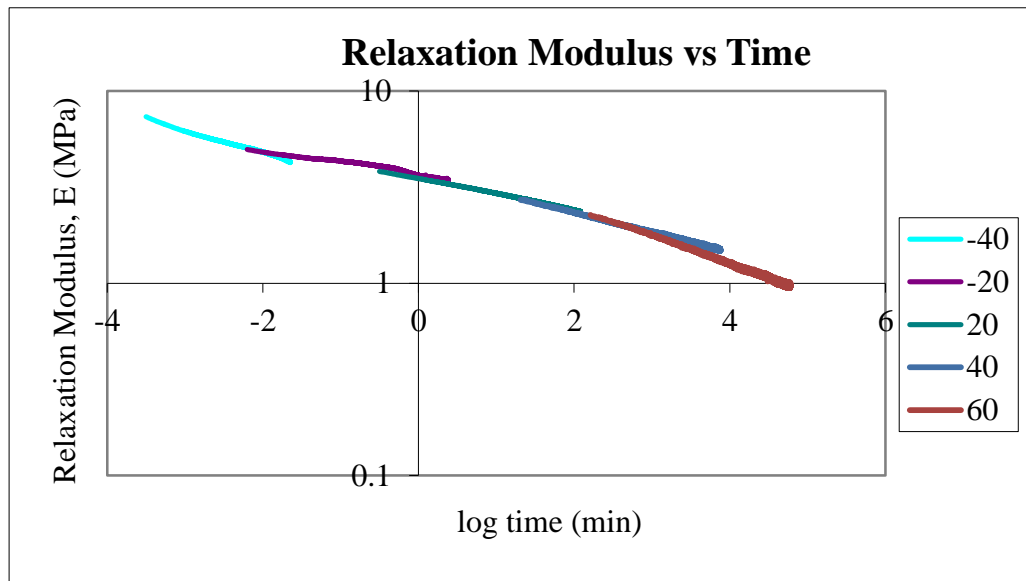


Figure 63 Master Curve obtained with mechanical tests (Relaxation modulus E vs reduced time)

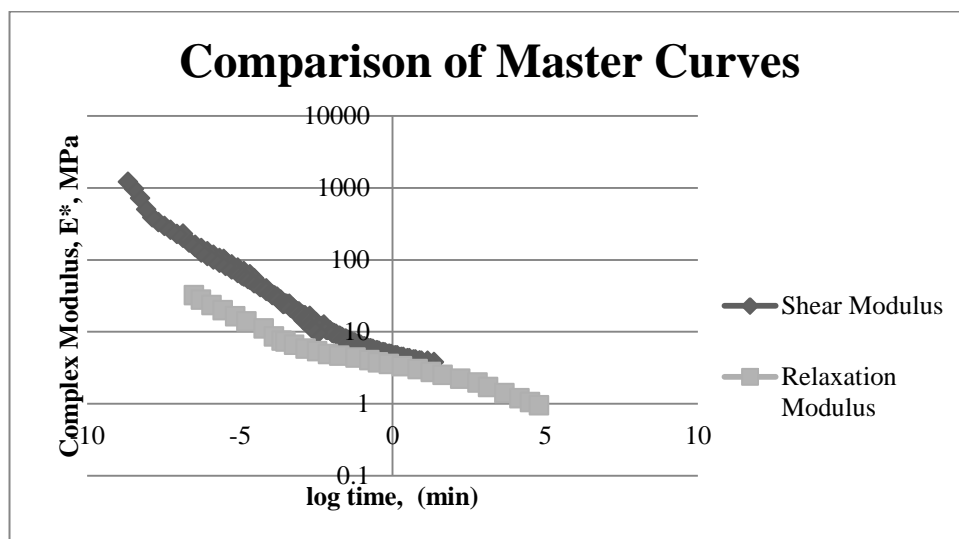


Figure 64 Comparison of master curves obtained both with rheometer and mechanical tests

From Figure 64, it can be calculated that the master curves from rheometer and mechanical tests were different at the beginning but they start to show consistence as time increases.

The comparison of the shift factors were given in Table 17. It was observed that, the difference between shift factors was increasing towards elevated temperatures.

Table 17 Comparison of shift factor calculated from each method

<u>T(°C)</u>	<u>$\log a_T$</u> <u>(RHEO.</u> <u>EXP.)</u>	<u>$\log a_T$</u> <u>(MECH.</u> <u>EXP.)</u>	<u>% ERROR</u>
-60°C	5.10	-	-
-40°C	3.15	3.00	5.0
-20°C	1.85	1.70	8.8
0°C	0.80	-	-
20°C	0.00	0.00	0.0
40°C	-0.70	-1.80	61.1
60°C	-1.27	-2.70	53.0

CHAPTER 4

CONCLUSION

Master curve estimations are important for prediction of propellant behavior under prolonged conditions. However, determination of these curves with mechanical tests consumes time and labor cost. In addition to these, to be able to perform the required tests, excess propellant mixtures are being prepared and this brings additional costs.

On the other hand, determination of master curves by rheometer is much simpler, cheaper and faster method. In this study, the conditions for master curve determination via rheometer were determined similar to mechanical test conditions, then the master curve was obtained with rheometer.

Moreover, the master curve from mechanical tests was estimated. Shift factors and WLF constants were also calculated. The modified WLF constants, Arrhenius shift factors and activation energies from both techniques were compared.

When the results were compared, since the deformation modes are different (tension in mechanical tests, and torsion in rheometer) it was concluded that there is no possible correlation between the two techniques directly. The master curve cannot be derived only by rheometer. The conventional mechanical tests should be used. At this point, it was concluded that, the rheometer data is significantly different from mechanical test data and the rheometer data is not reliable enough to completely reject mechanical test data.

For further studies, this study can be conducted for repeatability and both techniques can be compared each time. If the difference between two technique stays constant in

each study, a factor can be generated between two methods. This factor can further be used to determine criteria without conducting mechanical tests.

REFERENCES

Advisory Group for Aerospace Research & Development, *Structural Assessment of Solid Propellant Grains*, AGARD, **December 1997**.

Affens, W. A., *Ignition Studies, Part VII. The Determination of Autoignition by Hydrocarbon Fuels*, NTIS, **April 1974**, AD-778 – 998.

Asthana S. N., Divekar C. N., Khare R. R., Shrotri P. G., *Thermal Behavior of AP – Based CMDB Propellants With Stabilizers*, Defence Science Journal, 42, 3, **July 1992**, 201 – 204.

ASTM 1461 – 01 *Standard Test Method for Thermal Diffusivity by the Flash Method*.

ASTM E2716-09 *Standard test method for determining Specific Heat Capacity by Sinusoidal Modulated Temperature Differential Scanning Calorimetry*

ASTM E2716-09 *Standard test method for determining Specific Heat Capacity by Sinusoidal Modulated Temperature Differential Scanning Calorimetry*

ASTM Standard E 831-03, *Standard Test Method for Linear Thermal Expansion of Solid Materials by Thermomechanical Analysis*, **2003**.

Benson T., *Brief History of Rockets*, National Aeronautics and Space Administration, https://www.grc.nasa.gov/www/k-12/TRC/Rockets/history_of_rockets.html, last visited on 2015 September 15.

Billen J., PhD Thesis, San Diego State University, *Williams – Landel – Ferry and Vogel Fulcher Tamman Equations*, **2012**.

Bilyk S. R., Sheidler J. S., *Mechanical Response and Shear Initiation of Double-Base Propellants*, 13th International Detonation Symposium, **23 – 28 August 2009**.

Bozic V., *Effects of Burning Rate Modifiers on the Modified Polyvinyl Chloride – Based Propellants*, International Conference on High Energetic Materials and Dynamics of Ultrafast Reactive Systems, **16 – 18 June 2010**.

Brostow W., D'Souza N. A., *Creep and stress relaxation in a longitudinal polymer liquid crystal: Prediction of the temperature shift factor*, Journal of Chemical Physics, 110, 19, **May 1999**, 9706 – 9712.

Buswell H. J., PhD Thesis, University of Surrey, *An Investigation Into Mechanical Failure Of Composite Propellants*, **1975**.

Cai W., Thakre P., Yang Vigor, *A Model Of AP/HTPB Composite Propellant Combustion In Rocket – Motor Environments*, Combustion Science and Tech., 180, **2008**, 2143 – 2169.

Cerri S., Bohn M., A., Menke K., Galfetti L., *Ageing Behaviour of HTPB Based Rocket Propellant Formulations*, Central European Journal of Energetic Materials, 6(2), **2009**, 149 – 165.

Chaturvedi S., Dave P. N., *Solid Propellants: AP/HTPB Composite Propellants*, Arabian Journal of Chemistry, **December 2014**.

Davenas A., *Solid Rocket Propulsion Technology*, 1stEddition, France, **1993**, 329 – 331.

Davenas A., *Solid Rocket Propulsion Technology*, 1stEddition, France, **1993**, 415 – 416.

Dealy J., Plazck D., *Time – Temperature Superposition – A Users Guide*, *Rheology Bulletin*, 78, 2, **July 2009**.

Ferry J. D., *Viscoelastic Properties of Polymers*, 2nd Edition, **1970**.

Gurp, M., Palmen, J., *Time-Temperature Superposition for Polymer Blends*, *Rheology Bulletin*, 67, 1, **1998**, 5 – 8.

Herder G., Weterings F. P., Klerk W. P. C., *Mechanical Analysis On Rocket Propellants*, *Journal of Thermal Analysis and Calorimetry*, 72, **2003**, 921 – 929.

Hu M., PhD Thesis, Texas Tech University, *Rheological Responses of Polymer Materials With Different Architectures*, 2011.

Hunley J. D., *The History Of Solid – Propellant Roketry: What We Do and Do Not Know*, American Institute of Aeronautics and Astronautics, **1999**.

Jain S. R., *Solid Propellant Binders*, *J of Scientific & Industrial Research*, Vol 61, **November 2002**, 899 – 911.

Jeremic R., *Some Aspects of Time-Temperature Superposition Principle Applied for Predicting Mechanical Properties of Solid Rocket Propellants*, *Propellants, Explosives, Pyrotechnics*, 24, **1999** 221 – 223.

Jinsheng X., Xiong C., Hongli W., Jian Z., Changsheng Z., *Thermo-damage-viscoelastic constitutive model of HTPB composite*, *International Journal of Solids and Structures* 51, **2014**, 3209 – 3217.

Jones D. I. G., *Handbook of Viscoelastic Vibration Damping*, **2001**.

Kai D., Jianhong Y., Weiwei H., Fei C., Chaofeng L., Chengwu L., Hui Z., Yanjun W., *A new method to obtain shear modulus of solid propellant*, *Acta Astronautica*, 69, **2011**, 440 – 444.

Kakavas P. A., *Mechanical properties of propellant composite materials reinforced with ammonium perchlorate particles*, *International Journal of Solids and Structures*, 51, **2014**, 2019 – 2026.

Kakumanu L., Yadav N., Karmakar S., *Combustion Study of Composite Solid Propellants Containing Metal Phthalocyanines*, International Journal of Aerospace Sciences, 3(2), **2014**, 31 – 36.

Kishore K., Sunitha M. R., *Effect of Transition Metal Oxides on Decomposition and Deflagration of Composite Solid Propellant Systems: A Survey*, AIAA Journal, 17, 10 **1979**, 1118 – 1125.

Krevelen D. W., *Properties of Polymer, Correlations with Chemical Structure*, **1972**.

Kumari A., Mehilal, Jain S., Jain M. K., Bhattacharya B., *Nano-Ammonium Perchlorate: Preparation, Characterization, and Evaluation in Composite Propellant Formulation* J of Energetic Materials, 31, **2013**, 192 – 202.

Lakes, R. S., *Viscoelastic Solids*, **1999**.

Lieb R. J., Leadore M. G., *Time-Temperature Shift Factors for Gun Propellants*, Army Research Laboratory, **1993**.

Marques S. P. C., Creus G. J., *Computational Viscoelasticity*, XI, **2012**, 17.

Mehilal, Jawale L. S., Dey C., Gupta M., Bhattacharya B., *Effect of Experiment Environment on Calorimetric Value of Composite Solid Propellants*, Defence Science Journal, 63, 5, **September 2013**, 467-472.

Mehilal, Wani V. S., Jain S., Singh P. P., Bhattacharya B., *Prediction of Storage Life of Propellants Having Different Burning Rates Using Dynamic Mechanical Analysis*, Defence Science Journal, 62, 5, **September 2012**, 290 – 294.

Mehilal, Wani V. S., Jain S., Singh P. P., Bhattacharya B., *Studies On the Influence of Testing Parameters on Dynamic and Transient Properties Of*

Composite Solid Rocket Propellants Using a Dynamic Mechanical Analyzer, J. Aerosp. Technol. Manag., 1.4, 4, **2012**, 443 – 452.

Menard K. P., *Dynamic Mechanical Analysis: A Practical Introduction*, **2008**.

Merlette N., Pagnacco E., *Structural Dynamics Of Solid Propellants With Frequency Dependent Properties*, 12th European Conference on Space Structures, Materials & Environmental Testing, **July 2012**.

Musanic S. M., Suceca M., *Artificial Ageing Of Double Base Rocket Propellant Effect on Dynamic Mechanical Properties*, Journal of Thermal Analysis and Calorimetry, 96 (2), **2009**, 523 – 529.

Musanic S., Suceca M., *Dynamic Mechanical Properties of Artificially Aged Double Base Rocket Propellant and the Possibilities for the Prediction of Their Service Lifetime*, Central European Journal of Energetic Materials, 10, 2, **2013**, 225 – 244.

Muthiah Rm., Somasundaran U. I., Verghese T. L., Thomas V. A., *Energetics and Compatibility of Plasticizers in Composite Solid Propellants*, Def Sci J, 39, 2, **April 1989**, 147-155.

NATO Standardization Agency, STANAG 4507 PCS (Ed. 1) *Explosives, Physical/Mechanical Properties Stress Relaxation Test in Tension*, **Jan. 2002**.

NATO Standardization Agency, STANAG 4515 *Explosives: Thermal Characterization by Differential Thermal Analysis, Differential Scanning Calorimetry and Thermogravimetric Analysis*, **Aug. 2002**.

NATO Standardization Agency, STANAG 4525 (Ed. 1) *Explosives, Physical/Mechanical Properties, Thermomechanical Analysis for Determining the Coefficient of Linear Thermal Expansion (TMA)*, **October 2001**.

NATO Standardization Agency, STANAG 4540 (Ed. 1) *Explosives, Procedures for Dynamic Mechanical Analysis (DMA) and Determination of Glass Transition Temperature*, **Aug. 2002**.

Neviere R., *An Extension Of The Time–Temperature Superposition Principle To Non-Linear Viscoelastic Solids*, International Journal of Solids and Structures 43, **2006**, 5295 – 5306.

Okubo N., *Preparation of Master Curves by Dynamic Viscoelastic Measurements*. Hitachi High - Tech., **January 1990**.

Özkaya N., et al., *Fundamentals of Biomechanics: Equilibrium, Motion, and Deformation*, Mechanical Properties of Biological Tissues, 221 – 228, **2012**.

Petkovic J., Wali Amhamed., Mijin D., Uscumlic G., *The Influence of Bonding Agents in Improving Interactions in Composite Propellants, Determined Using the FTIR Spectra*, Scientific Technical Review, LIX, 3 – 4, **2009**.

Petrou A. L., Roulia M., Tampouris K., *The Use Of Arrhenius Equation In The Study Of Deterioration And Cooking Of Foods – Some Scientific and Pedagogic Aspects*, Chemistry Education: Research and Practice In Europe, 3, 1, **2002**, 87 – 97.

Polacco G., Vacin O., J., Biondi D., Stastna J., Zanzotto L., *Dynamic Master Curves of Polymer Modified Asphalt from Three Different Geometries*, Appl. Rheology, 13, **2003**, 118 – 124.

Rocco J. A. F. F., Lima J. E. S., Frutuoso A. G., Iha K., Ionashiro M., Matos J. R., Suárez-Iha M. E. V., *TG Studies Of A Composite Solid Rocket Propellant Based On HTPB-Binder*, Journal of Thermal Analysis and Calorimetry, 77, **2004**, 803 – 813.

Rodic V., Petric., *The Effect Of Additives on Solid Rocket Propellant Characteristics*, Scientific Technical Review, 54, 3 – 4, **2004**.

Ronan S., Alshuth T., Jerrams S., Murphy N., *Long-term Stress Relaxation Prediction For Elastomers Using The Time–Temperature Superposition Method*, *Materials and Design*, 28, **2007**, 1513 – 1523.

Rowe G. M., Sharrock M. J., *Development of Standard Techniques for the Calculation of Master Curves for Linear – Viscoelastic Materials*, The 1st International Symposium on Binder Rheology And Pavement Performance, 13-15, **2000**.

Roylance D., *Engineering Viscoelasticity*, Department of Materials Science and Engineering Massachusetts Institute of Technology, **October 2001**.

Saçak M., *Polimer Kimyası*, Chapter 2, **2002**.

Sakovich G. V., *Design Principles of Advanced Solid Propellants*, *Journal of Propulsion And Power*, 11, 4, **July – August 1995**, 830 – 837.

Santhosh G., Venkatachalam S., Ninan K. N., *High Energy Oxidizers for Advanced Solid Propellants and Explosives*, *Advances in Solid Propellant Technology*, 1st International HEMS1 Workshop, Ranchi, India, **2002**, 87 – 106.

Sarner S. F., *Propellant Chemistry*, **1966**.

Strahle W. C., Handley J. C., Milkie T. T., *Final Report On Mechanisms Of Composite Solid Propellant Combustion*, Naval Weapons Center, **1972**.

Sutton G. P., Biblarz O., *Rocket Propulsion Elements*, 8th Edition, **2010**.

Tanjore D., Ms Thesis, North Carolina State University, *Application for Brookfield Viscometers: Viscoelastic Property Determination*, **2005**.

Villar L. D., Silva R. F., Diniz M. F., Takahashi M. F. K., Rezende L. C., *The Role of Anti – Oxidant on Propellant Binder Reactivity During*

Thermal Aging, J. Aerosp. Technol. Manag., 2, **May – Aug 2010**, 163 – 168.

Wallace H. Boggs, *Autoignition – A Liquid Propellant Explosive Potential Limiting Phenomena*, The Space Congress Proceedings, **April 1976**.

Ward I. M., Sweeney J., *The Mechanical Properties of Solid Polymers*, 2nd Edition, **1977**.

Ward J. R., *Determination Of Heat Capacities Of Gun Propellants By Differential Scanning Calorimetry*, Analytical Calorimetry, New York, **1977**, 143 – 153.

Wingborg N., *Increasing the tensile strength of HTPB with different isocyanates and chain extenders*, Polymer Testing, 21, **2002**, 283 – 287.

Wingborg N., Ms Thesis, KHT Royal Institute of Technology, *Improving the Mechanical Properties of Composite Rocket Propellants*, **2004**.

Witzack M. W., Arizona State University Research Project, *Development Of A Master Curve (E^*) Database For Lime Modified Asphaltic Mixtures*, **July 2004**.

Yılmaz O., Ms Thesis, Middle East Technical University, *Service Life Assessment Of Solid Rocket Propellants Considering Random Thermal And Vibratory Loads*, **August 2012**.

Zhang J. W., Zhi S., Sun B., *Estimation Of Thermophysical Properties Of Solid Propellants Based on Packing Model*, Sci China Tech Sci, 56, 12, **December 2013**, 3055 – 3069.